_____

Associate Prof. Dipl.-Ing. Dr.techn. Andreas Limbeck

TECHNISCHE UNIVERSITÄT WIEN
Vienna University of Technology

Diplomarbeit

Development of ICP-based methods for laterally resolved stoichiometry determination of $Li_{7-3x}Al_xLa_3Zr_2O_{12}$ garnets

ausgeführt am Institut für
Chemische Technologien und Analytik
der Technischen Universität Wien

unter der Anleitung von
Associate Prof. Dipl.-Ing. Dr.techn. Andreas Limbeck
Univ.Prof. Dipl.-Phys. Dr.rer.nat. Jürgen Fleig
Kolleg. Dipl.-Ing. Maximilian Bonta, BSc

durch
Stefan Smetaczek
Kimmerlgasse 15
1110 Wien

Wien, im November 2016

_____

Stefan Smetaczek, BSc

Abstract

The performance and safety of currently used Li-ion batteries is limited by the utilized instable organic electrolytes. Therefore, replacing these liquid electrolytes by inorganic solid ion conductors is of major interest. Due to their high Li-ion conductivity and chemical and electrochemical stability, $Li_7La_3Zr_2O_{12}$ (LLZO) garnets are among the most promising candidates for future all solid state Li-ion batteries. Since the highly conductive cubic modification of LLZO can be stabilized by the introduction of certain supervalent cations such as Al^{3+}, especially doped LLZO variants like $Li_{7-3x}Al_xLa_3Zr_2O_{12}$ have attracted attention.

Despite extensive research in recent years, the reproducible synthesis of highly conductive LLZO remains challenging. Processes involved in the synthesis as well as the relationship between chemical composition and conduction behavior of the resulting LLZO garnets are still not completely understood. To investigate those, an analytical method capable of detecting and quantifying all metals of the material including Li is needed. The coupling of ICP-OES or ICP-MS to laser ablation (LA) not only fulfills this requirement, but also enables spatially resolved direct solid analysis without time-consuming sample preparation.

In this work, the development of an ICP-based method for the laterally resolved stoichiometry determination of $Li_{7-3x}Al_xLa_3Zr_2O_{12}$ garnets is described. Since reliable quantification of LA measurements is only possible using matrix-matched calibration standards, the preparation of suitable LLZO standards as well as the determination of their chemical composition was required beforehand.

Homogeneous LLZO standards were successfully prepared by pressing ground LLZO powders with varying Al content into pellets. The stoichiometry of the utilized powders was determined using borax fusion for sample digestion in combination with ICP-OES analysis. Using these pressed LLZO pellets as standards for signal quantification, LA-ICP-MS as well as LA-ICP-OES experiments were performed. Thereby, two different calibration strategies were applied: A conventional univariate external calibration approach in combination with the use of La as internal standard and an internal-standard independent calibration strategy based on the normalization of the sum of all metal oxides to 100 wt%.

Results show that LA-ICP-MS is not suitable for the quantitative analysis of LLZO due to a lack of the required precision of the Li-measurement, which is probably caused by mass discrimination due to space-charge effects. In contrast to that, a LA-ICP-OES method capable of quantitative and spatially resolved analysis of $Li_{7-3x}Al_xLa_3Zr_2O_{12}$ could be found. Although both calibration strategies provide similar results, the 100 wt% normalization approach is superior to the conventional external calibration due to the capability of complete stoichiometry determination.

To investigate possible changes of the chemical composition during the LLZO-synthesis, starting materials, intermediates and product of a "$Li_{6.4}Al_{0.2}La_3Zr_2O_{12}$" synthesis were analyzed using borax fusion and ICP-OES measurement. The results of the experiments indicate the loss/incorporation of CO_2 and/or moisture during the different stages of the synthesis process

as well as a significant loss of Li during sintering. Further analyses of different LLZO samples with varying Al contents showed a significant Al-incorporation during sintering for samples with an intended Al concentration close to zero.

For the investigation of local variations of the chemical composition, two-dimensional elemental distribution images of whole "$Li_{6.4}Al_{0.2}La_3Zr_2O_{12}$" pellets were created during method development. The LA-ICP-MS experiments revealed local variations of the Al content up to 54% relatively, as well as Li-rich phases and C-impurities.

Kurzfassung

Die Leistungsfähigkeit und Sicherheit aktuell verwendeter Li-Ionen-Akkumulatoren ist durch den Einsatz instabiler organischer Elektrolyten beschränkt. Daher ist vom großem Interesse, diese Flüssigelektrolyten durch feste anorganische Ionenleiter zu ersetzen. $Li_7La_3Zr_2O_{12}$ (LLZO) Granate zählen aufgrund ihrer hoher Li-Ionen Leitfähigkeit sowie chemischer und elektrochemischer Stabilität zu den vielversprechendsten Kandidaten für zukünftige Li-Ionen-Festkörperakkumulatoren. Da die hochleitfähige kubische Modifikation von LLZO durch Einbringen von bestimmten mehrfach geladenen Ionen wie Al^{3+} stabilisiert werden kann, finden dabei vor allem dotierte LLZO Varianten wie $Li_{7-3x}Al_xLa_3Zr_2O_{12}$ Beachtung.

Trotz intensiver Forschung in den letzten Jahren bleibt die reproduzierbare Synthese von hochleitfähigem LLZO eine Herausforderung. Sowohl die an der Synthese beteiligten Prozesse als auch die Zusammenhänge von chemischer Zusammensetzung und Leitfähigkeit sind dabei noch nicht vollständig verstanden. Um diese untersuchen zu können, ist eine analytische Methode erforderlich, die in dem Material enthaltenen Metalle einschließlich Li detektieren und quantifizieren kann. Die Kopplung von ICP-OES oder ICP-MS mit Laserablation (LA) erfüllt diese Anforderung nicht nur, sondern ermöglicht außerdem räumlich aufgelöste direkte Feststoffanalysen ohne zeitaufwändige Probenvorbereitung.

In dieser Arbeit ist die Entwicklung einer auf ICP basierenden Methode für die ortsaufgelöste Bestimmung der Stöchiometrie von $Li_{7-3x}Al_xLa_3Zr_2O_{12}$ Proben beschrieben. Da eine verlässliche Quantifizierung von LA-Messungen nur unter Verwendung von matrixangepassten Standards möglich ist, war zuvor die Herstellung geeigneter LLZO Standards und die Bestimmung derer chemischen Zusammensetzung erforderlich.

Homogene LLZO Standards wurden erfolgreich durch Pressen gemahlener LLZO Pulver mit unterschiedlichen Al-Gehalten hergestellt. Die Stöchiometrie der verwendeten Pulver wurde mittels Borax-Schmelzaufschluss und ICP-OES Analyse bestimmt. Die hergestellten LLZO Presslinge wurden als matrixangepasste Standards für die Signalquantifizierung von LA-ICP-MS und LA-ICP-OES Messungen verwendet. Dabei wurden zwei verschiedene Kalibrationstrategien angewandt: Einerseits herkömmliche externe Kalibration in Kombination mit der Verwendung von La als interner Standard, sowie andererseits ein Kalibrationsansatz, der keinen internen Standard erfordert und auf der Normalisierung der Summe aller Metalloxide auf 100 wt% basiert.

Die Ergebnisse zeigen, dass LA-ICP-MS nicht für die quantitative Analyse von LLZO geeignet ist. Ursache dafür ist die fehlende Präzision bei der Li-Bestimmung, welche vermutlich auf Massendiskriminierung aufgrund von Raumladungseffekten zurückzuführen ist. Im Gegensatz dazu konnte eine LA-ICP-OES Methode gefunden werden, die eine quantitative und räumlich aufgelöste Analyse von $Li_{7-3x}Al_xLa_3Zr_2O_{12}$ ermöglicht. Obwohl beide Kalibrationsstrategien ähnliche Ergebnisse liefern, ist die Methode der 100 wt% Normalisierung der herkömmlichen externen Kalibration überlegen, da sie die vollständige Bestimmung der Stöchiometrie erlaubt.

Um Veränderungen in der chemischen Zusammensetzung während einer LLZO Synthese festzustellen, wurden die Edukte, Intermediate und das Endprodukt einer "$Li_{6.4}Al_{0.2}La_3Zr_2O_{12}$" Synthese mittels Schmelzaufschluss und ICP-OES untersucht. Die Ergebnisse der Experimente deuten auf Verlust bzw. Aufnahme von CO_2 und/oder Feuchtigkeit während verschiedener Syntheseschritten sowie einem signifikanten Li-Verlust während des Sinterns hin. Weitere Analysen von LLZO Proben mit unterschiedlichem Al-Gehalt zeigen eine signifikante Al-Aufnahme während des Sinterns für jene Proben, die anfänglich nahezu frei von Al sind.

Zur Untersuchung lokaler Variation der chemischen Zusammensetzung wurden während der Methodenentwicklung zweidimensionale Elementverteilungsbilder ganzer "$Li_{6.4}Al_{0.2}La_3Zr_2O_{12}$" Tabletten erstellt. Die LA-ICP-MS Experimente zeigen relative lokale Variationen des Al-Anteils von bis zu 54% sowie Li-reiche Phasen und C-Verunreinigungen.

Danksagung

An dieser Stelle möchte ich mich bei all Jenen bedanken, die mich bei der Anfertigung dieser Diplomarbeit unterstützt und motiviert haben.

Zuallererst gebührt Andreas Limbeck mein Dank, der mich in seine Forschungsgruppe aufgenommen und meine Arbeit stets mit seinem Fachwissen begleitet hat. Seine Unterstützung und seine unzähligen hilfreichen Anregungen haben wesentlich zu den Ergebnissen dieser Arbeit beigetragen. Selbiges gilt für Maximilian Bonta, der mit größter Geduld all meine Frage beantwortet und mir bei einigen Problemen entscheidend weitergeholfen hat. Für eure Mühen und die ausgezeichnete Betreuung möchte ich mich ganz herzlich bedanken.

Auch den restlichen Mitgliedern der Arbeitsgruppe Limbeck gilt für das ausgesprochen gute Arbeitsklima und die schöne gemeinsame Zeit mein Dank. Insbesondere möchte ich mich bei Felix Horak und Winfried Nischkauer bedanken, die mir bei Schwierigkeiten stets mit großer Hilfsbereitschaft zur Seite standen. Ein besonderer Dank geht auch an András Hegyessy, der durch die Entwicklung des verwendeten Schmelzaufschlussverfahrens eine wertvolle Vorarbeit für meine Diplomarbeit geleistet hat.

Außerdem möchte ich mich herzlich bei Jürgen Fleig bedanken, der es überhaupt erst möglich gemacht hat, dass ich an diesem interessanten Thema arbeiten durfte. Seiner gesamten Forschungsgruppe, insbesondere Stefanie Taibl und Andreas Wachter-Welzl, möchte ich für die ausgesprochen gute und produktive Zusammenarbeit danken.

Auch den Kollegen vom Fachbereich Chemie und Physik der Materialen an der Paris-Lodron Universität Salzburg möchte ich für die gelungene Kooperation danken. Mein besonderer Dank gilt Reinhard Wagner, der alle in dieser Arbeit untersuchten Proben hergestellt hat.

Dank gebührt auch all meinen Freunden und Studienkollegen, die mich in den letzten Jahren begleitet und dabei stets mental unterstützt und motiviert haben. Danke für die schöne gemeinsame Zeit.

Abschließend möchte ich mich von ganzem Herzen bei meiner Familie bedanken, denn ohne sie wäre dieses Studium niemals möglich gewesen. Danke, dass ihr immer an mich geglaubt und mich sowohl finanziell als auch auf jede andere denkbare Weise unterstützt habt. Danke, dass ihr immer für mich da wart.

Table of contents

1   Introduction

Due to the rapid development of portable electronic devices and electric cars, more and more powerful batteries are needed. Among the known batteries are Li-based the most promising to face the upcoming challenges, because they offer the highest cell potential and volumetric as well as gravimetric energy density. [1]

Most rechargeable Li-ion batteries now in use employ electrolytes composed of organic solvents or polymers with a dissolved Li-salt. [2] However, these electrolytes have numerous unwanted properties: They are flammable, have poor electrochemical stability and a limited temperature range of operation, exhibit leakage, and pose health hazards. Therefore, solid state electrolytes are being considered to replace organic polymer-based electrolytes with the advantages of battery miniaturization, high-temperature stability, higher energy density, and greater battery safety. [3]

$Li_7La_3Zr_2O_{12}$ (LLZO) is a Li-ion conducting oxide with garnet-type structure, which has attracted much scientific attention in the last years. Beside the high Li-ion conductivity (10^{-3} to 10^{-4} S cm^{-1} at ambient temperature), the high mechanical, thermal, chemical, and electrochemical stability suggest that LLZO is a promising solid electrolyte for all kinds of Li-based rechargeable batteries, including "Beyond Li-Ion Battery" concepts such as Li-air or Li-S batteries. [3-5]

LLZO crystallizes in two different polymorphs: A low-temperature tetragonal (space group: $I4_1/acd$, No. 142) [6] and a high-temperature cubic modification (space group: $Ia\bar{3}d$, No. 230) [7]. For use as a Li-ion conductor, the cubic polymorph is much more desirable as its Li-ion conductivity is two orders of magnitude higher than for that tetragonal polymorph. [3, 6, 8] Although the cubic modification of pure LLZO is not stable at room temperature, it can be stabilized by the introduction of supervalent cations. In this matter, the most promising cations are Al and Ga, generally substituted on the Li sites. [8-10]

Although LLZO has been studied extensively in recent years, the reproducible synthesis of garnets with high Li-ion conductivity remains a challenge. The reasons for these variations of the conduction behavior are mostly unknown. However, connections with different chemical compositions of the samples due to unknown aspects of the synthesis process are obvious. Since the LLZO synthesis involves sintering at high temperature, phenomena such as Li_2O loss and diffusion processes are to be expected, which results in samples with unknown and potentially inhomogeneous chemical composition. In order to obtain information about the processes involved in the synthesis as well as to investigate the relationship between chemical composition and conduction behavior, a measurement method capable of the quantitative and spatially resolved analysis of LLZO samples is required.

Inductively coupled plasma optical emission spectrometry (ICP-OES) and inductively coupled plasma mass spectrometry (ICP-MS) are both widely used methods within the field of inorganic trace analysis. The ease of use combined with the multi-element capability, high dynamic range and the capability of trace analysis (or even ultra-trace analysis in case of ICP-MS) makes ICP-OES and -MS worthwhile methods for a large number of applications. Unlike other

analytical methods widely used for elemental analysis, such as x-ray based methods like x-ray fluorescence spectroscopy (XRF spectroscopy) and electron probe micro analysis (EPMA), ICP-OES and -MS are capable of detecting and quantifying Li, which makes them particularly suitable for the analysis of LLZO.

One of the biggest drawbacks of ICP-OES and -MS is that solid samples have to be converted into a liquid prior to analysis. Since many materials of interest, including oxides like LLZO, are not directly soluble in common solvents, often rigorous treatment is required for sample dissolution. Commonly used sample digestions methods include treatment with hot mineral acids and high-temperature fusion with reagents such as sodium carbonate or sodium tetraborate (borax). As a result, the sample preparation is usually very time-consuming. Additionally, potential errors are introduced due to the various sample digestion steps (e.g., analyte-loss by volatilization), which limits the accuracy of the analysis.

By coupling of ICP-OES or -MS with laser ablation (LA), direct sampling of solids becomes possible. Therefore, time-consuming and error-prone digestion methods are no longer required for the measurement. Furthermore, spatially resolved analysis can be carried out, which enables the investigation of the elemental distributions.

One of the most challenging aspects of LA-ICP-OES and LA-ICP-MS analyses is the capability of providing reliable quantitative information. The difficulty is that the detected signal intensities are usually not representative for the elemental composition of the investigated sample. This is caused by elemental fractionation during the ablation process, the transport of the aerosol into the ICP, and the processes in the ICP itself. In addition, the ablation behavior is dependent on the sample matrix, which means that the amount of analyte ablated changes due to different matrices. Since the mass load of the plasma affects the plasma conditions, this also changes the vaporization, atomization and ionization efficiencies of the analytes. [11]

Due to elemental fractionation and sample-related matrix effects, the signal quantification of LA-ICP-OES and LA-ICP-MS measurements often requires standards being similar to the samples. Because appropriate certified reference materials (CRMs) are not available for every type of sample, the in-house preparation of matrix-matched standards is usually required for calibration. However, such standards can be difficult to obtain or fabricate. Techniques used for the preparation of matrix-matched standards include: mixing and pressing with or without a binder, fusion with borate, or embedding in a polymer resin. [11, 12]

During this work, an ICP-OES method for the elemental analysis of Al-substituted LLZO ($Li_{7-3x}Al_xLa_3Zr_2O_{12}$) samples was developed. To transfer the samples to liquid form, a specific digestion method including a borax fusion was used. Beside sintered LLZO garnets, also corresponding starting materials and intermediates were analyzed to investigate possible changes of the chemical composition during the LLZO synthesis.

Furthermore, spatially resolved analysis of Al-substituted LLZO samples was carried out using LA-ICP-MS and LA-ICP-OES. Two-dimensional elemental distribution images of whole LLZO pellets were obtained, with both sample surfaces as well as cross-sections of the pellets being investigated.

In a final step, a calibration strategy for the quantification of the LA-ICP-MS and LA-ICP-OES measurements was developed. To ensure matrix-matched standards with constant chemical composition, different LLZO powders with varying Al content were pressed into pellets. After the chemical compositions have been determined by digestion and ICP-OES, these pellets were used for quantification of the signal intensities obtained during the LA measurements. Therefore, two different calibration approaches were applied. On the one hand, conventional univariate external calibration combined with the use of La as internal standard was used. On the other hand, an internal-standard independent calibration strategy presented by Liu et al [13] was applied, which is based on the normalization of the sum of all metal oxides to 100 wt%.

2   Theoretical background

2.1   Li₇La₃Zr₂O₁₂ (LLZO)

2.1.1   Pure LLZO

The Li-conductive oxide $Li_7La_3Zr_2O_{12}$ (LLZO) with garnet-like structure is a solid electrolyte material for Li-based battery applications. It provides high Li-ion conductivity of 10^{-3} to 10^{-4} S cm^{-1} at ambient temperature, a Li$^+$ transference number close to unity ($t_{Li+} \sim 1$), superior chemical stability against high voltage cathodes and electrochemical inertness in a wide potential window up to 6 V. [3-5]

Pure LLZO crystallizes in a low-conductivity tetragonal and a high-conductivity cubic polymorph. The low-temperature tetragonal modification shows space group $I4_1/acd$ (No. 142). This structure type is described as garnet-related framework composing of two types of dodecahedral LaO_8 plus octahedral ZrO_6. The Li atoms occupy three crystallographic sites in the interstices of this structure: The tetrahedral 8*a* site and the distorted octahedral 16*f* and 32*g* sites. [6] A graphical representation of this structure is displayed in Figure 1.
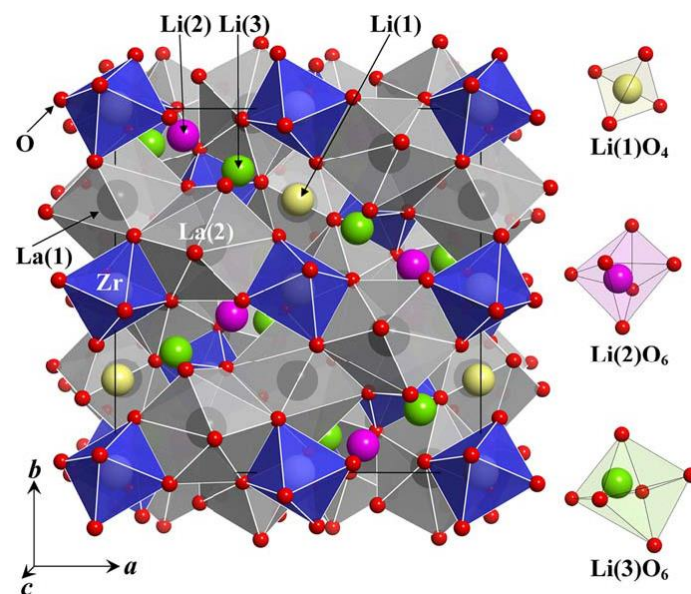

Figure 1: Crystal structure of tetragonal $Li_7La_3Zr_2O_{12}$ with space group I41/acd [6]

The high-temperature cubic modification crystallizes in space group $Ia\bar{3}d$ (No. 230). As shown in Figure 2, this modification has a garnet framework structure composing of dodecahedral LaO_8 and octahedral ZrO_6. The Li atoms occupy two types of crystallographic sites in the interstices of the structure: The tetrahedral 24*d* site and the distorted octahedral 96*h* site. In contrast to tetragonal polymorph, the cubic high-conductivity modification exhibits a disorder in the Li-distribution (Li-sites partially occupied). The Li atomic arrangement, which should correspond to the Li-ion migration pathways, shows a three-dimensional network structure with short Li-Li distance, which may be related to the good Li-ion conductivity of the garnet. [7]
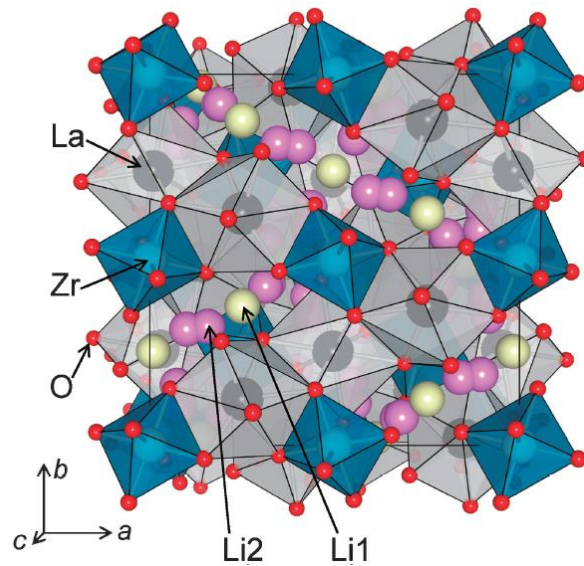
Figure 2: Crystal structure of cubic Li$_7$La$_3$Zr$_2$O$_{12}$ with space group Ia$\bar{3}$d [7]

2.1.2   Al-substituted LLZO (Li$_{7-3x}$Al$_x$La$_3$Zr$_2$O$_{12}$)

The highly conductive cubic modification of LLZO, which is not stable at room temperature for pure LLZO, is stabilized by supervalent substitution. Al^{3+} is one of the most promising candidates among the supervalent cations capable of this stabilization. The Al-substitution of LLZO results in the formula unit Li$_{7-3x}$Al$_x$La$_3$Zr$_2$O$_{12}$. [8, 9]

Because Al^{3+} is incorporated at the Li$^+$ sites, the substitution causes a reduction of the Li$^+$ content due to charge compensation, which leads to the introduction of vacancies into the Li-sublattice. These vacancies reduce the free energy advantage of complete ordering on the Li-sublattice, eventually leading to disorder and a transition to cubic symmetry. [14]

2.2   ICP-OES

2.2.1   Principle and overview

Inductively coupled mass optical emission spectrometry (ICP-OES) is a widely used analytical technique for the determination of trace elements. It features multi-element capability (over 70 elements including P and S), low chemical interference, a stable and reproducible signal as well as low detection limits for most elements (0.1 – 100 ng g^{-1}) and a wide linear dynamic range (four to six orders of magnitude). [15]

ICP-OES uses a high-temperature plasma produced through electromagnetic induction for generation of optical emission. A plasma is an electrically conducting gaseous mixture, which contains a significant concentration of ions and electrons. In ICP-OES, the sample is introduced as a gas, vapor, or aerosol of fine droplets or solid particles into the plasma. There the particles, molecules and atoms are atomized, excited and ionized. As the excited species

rapidly relax back to lower states, ultraviolet and visible line spectra arise, which are monitored and used for qualitative and quantitative elemental analysis. Therefore, the emitted radiation is dispersed according to its wavelength and the intensities of emission lines characteristic for specific atoms (or ions) are measured.

There are two types of ICP-OES devices: Sequential and multichannel instruments. Sequential systems move from the emission line for one element to that of the next. In contrast, multichannel instruments can detect the intensities of emission lines for several elements simultaneously, which enables fast determination of a large number of elements.

In ICP-OES different types of diffraction gratings are used for dispersion of the emitted radiation. Cerny-Turner design, Rowland circle geometry or Echelle optics can be employed. For detection of the light, photomultiplier tubes (PMT) as well as charge coupled devices (CCDs) and charge injection devices (CIDs) are used. [16]

Most ICP-OES devices used today are equipped with an Echelle polychromator and a CCD or CID array detector. With this set-up, the full emission spectrum can be measured simultaneously, allowing the analysis of numerous elements within a short time scale. A schematic of such an instrument, which also has been used in this work, is shown in Figure 3.
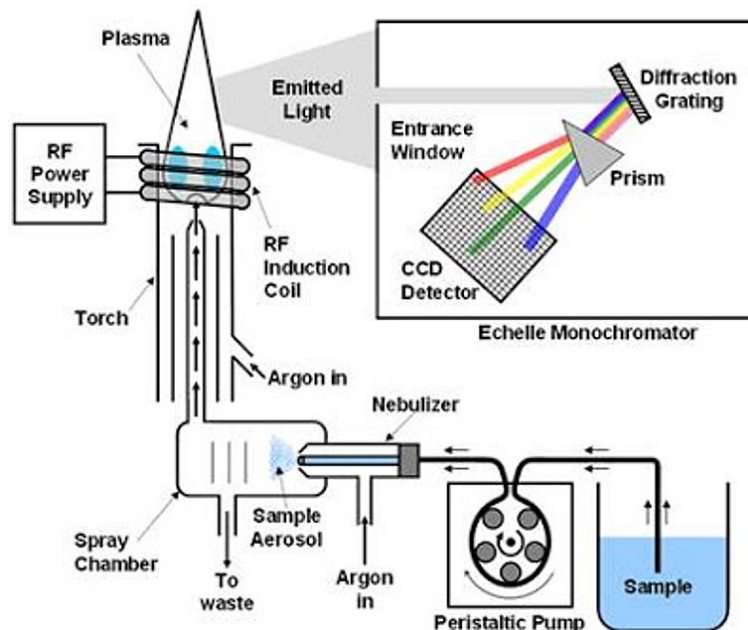

Figure 3: Schematic of a simultaneous type ICP optical emission spectrometer with echelle optics and a CCD detector, equipped with a pneumatic nebulizer and a spray chamber for the sample introduction of liquids (Source: http://www.rohs-cmet.in/content/icp-oes; Access date: October 10, 2016)

2.2.2 Sample introduction

The most commonly used devices for liquid sample introduction in ICP-OES (and ICP-MS) are nebulizers. Different kinds of pneumatic (e.g., concentric, cross-flow, Babington) as well as ultrasonic nebulizers are used. The most common type is the pneumatic concentric glass nebulizer, which is shown in Figure 4. The sample solution is usually supplied by means of a peristaltic pump. Droplet separation after nebulization can be carried out in different kinds of spray chambers. [15]

Beside slurry nebulization, the most often used techniques for the introduction of solid samples into the plasma are arc and spark ablation, laser ablation and electro-thermal vaporization. [16]
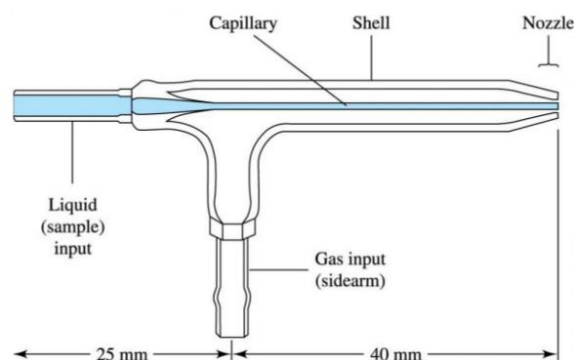

Figure 4: Concentric nebulizer [16]

2.2.3 Inductively coupled plasma (ICP)

The inductively coupled plasma (ICP) is one of the most important excitation and ionization sources in the field of inorganic elemental analysis. Figure 5 shows a schematic drawing of a typical ICP source, the so-called plasma torch.

The plasma torch consists of three concentric tubes made of quartz glass trough which streams of Ar gas flow. The sample aerosol carried by the inner Ar flow ($0.5 - 1.5$ l min^{-1}) is introduced into the center of the plasma jet. The outer gas flow ($11 - 14$ l min^{-1}), usually introduced tangentially, sustains the plasma and cools the plasma confinement tube to prevent it from melting. The intermediate tube contains the auxiliary gas ($0.5 - 2$ l min^{-1}), which has the function to lift the plasma away from the inner tubes. [17]

Surrounding the top of the largest tube is a water-cooled induction coil. It is powered by a HF generator, which radiates $700 - 2000$ W power at a frequency of 27.12 or 40.68 MHz. [18] For igniting the plasma, a spark of a Tesla coil is used to ionize the first Ar atoms. The produced ions and electrons interact with the fluctuating magnetic field produced by the induction coil. By collisions more and more atoms get ionized and the plasma is formed, which reaches typically a temperature between 5500 and 8000 K depending on the HF energy and the applied gas flows. [16]
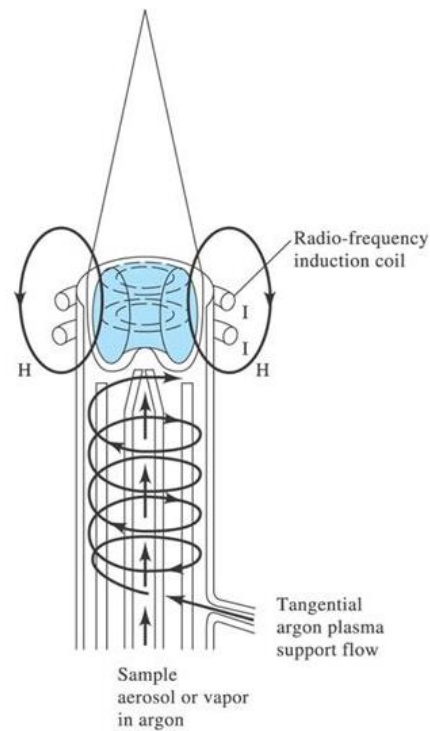
Figure 5: Schematic of an ICP torch [16] (adapted)

2.2.4 Echelle monochromator

As shown in Figure 6, an Echelle monochromator contains two dispersive elements arranged in series. In a first step, the radiation is dispersed by an Echelle grating, a low period reflective grating designed for use in the high diffraction orders. Then, a second, perpendicularly mounted dispersing element (prism or grating) separates the overlapping diffraction orders. This leads to a two-dimensional pattern of the spectrum, which can be projected onto an array detector like a CID detector allowing the measurement of the full spectrum in one step.
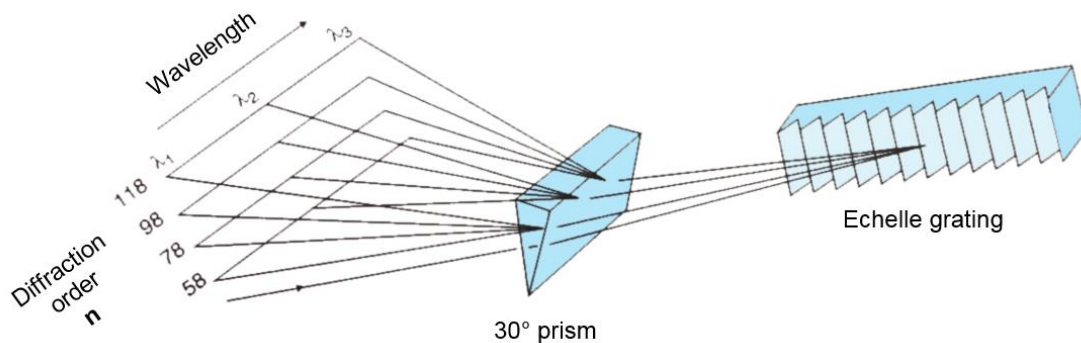

Figure 6: Echelle monochromator [16] (adapted)

2.2.5 CID detector

A charge injection device (CID) is a solid-state array detector consisting of small photosensitive elements arranged either linearly or as a two-dimensional pattern on a single semiconductor chip. CIDs form together with charge coupled devices (CCDs) the class of charge transfer devices (CTDs), which feature high dynamic ranges and good sensitivity compared to photodiode arrays. [19]

A schematic of a pixel for CID detector is shown in Figure 7. Photons falling on the n-type silicon substrate produce electron-hole pairs. By applying a negative potential to metal electrodes, the holes generated in a given region are collected and trapped just below the insulating layer. The created amount of charge is measured by sensing changes in voltage as the charge is shifted between the adjacent electrodes. [20]
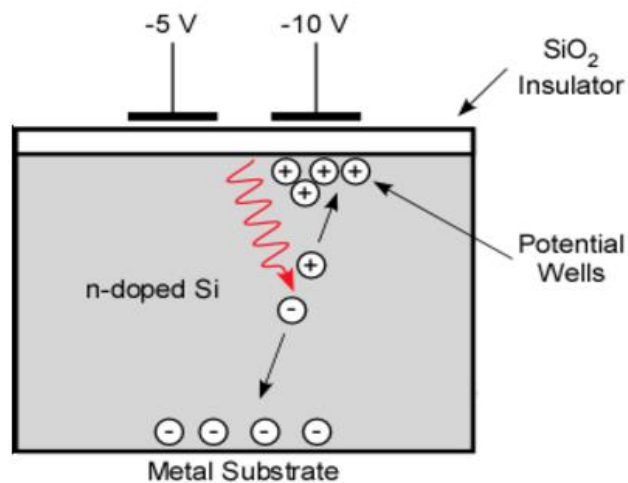

Figure 7: Cross-sectional diagram of a pixel for a CID detector [19] (adapted)

2.3 ICP-MS

2.3.1 Principle and overview

Inductively coupled mass spectrometry (ICP-MS) is one of the most important techniques for elemental analysis. It is routinely deployed in many diverse research fields such as earth, environmental, life, and forensic sciences, as well as food, material, chemical, semiconductor, and nuclear industries. [21]

ICP-MS features short measurement times between seconds and minutes, very low detection limits in the region of 10^{-9} to 10^{-12} g g^{-1}, multi-element capability (78 elements) and a wide dynamic range over approximately eight orders of magnitude. [18] Additionally, isotope analyses can be carried out, which are barely accessible for non-mass spectrometric techniques.

A schematic overview of an ICP-MS is presented in Figure 8. For sample introduction, different kinds of techniques can be used, which were already described earlier in section 2.2.2. However, compared to ICP-OES, lower sample introduction rates are desired in ICP-MS. After the sample aerosol is atomized, excited, and ionized in the inductively coupled plasma (see section 2.2.3), the generated ions are transferred into the high vacuum of the mass spectrometer via an interface. There, the ion beam is at first focused by ion optics. Afterwards the ions are separated according to their mass-to-charge ratios m/z by a mass analyzer and detected by a transducer.
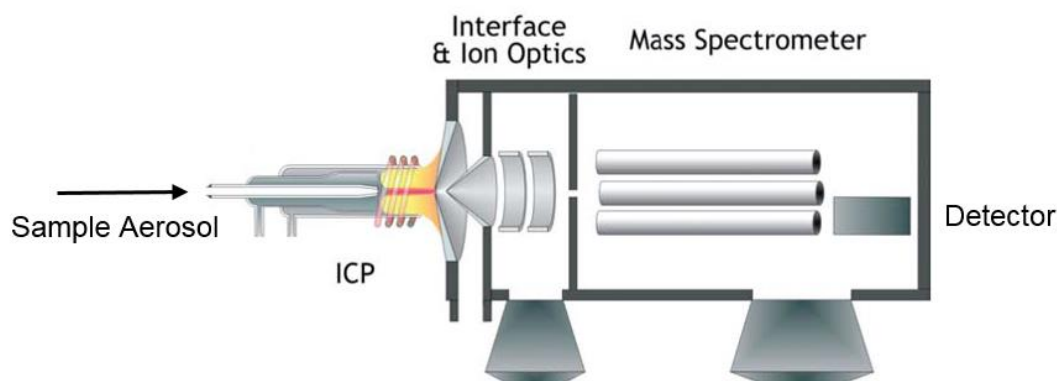

Figure 8: Schematic set-up of an ICP-MS [22] (adapted)

Most ICP-MS instruments used today are equipped with a quadrupole mass analyzer, but also sectorfield and time-of-flight mass spectrometers are used. For the detection of the ions mostly electron multipliers are applied. [16]

For the presented experiments, a quadrupole ICP-MS instrument with a channel electron multiplier (CEM) has been used. Thus, only this configuration will be discussed in more detail.

2.3.2   Vacuum interface

The interface region in the ICP-MS couples the plasma torch, which operates at atmospheric pressure with the mass spectrometer that requires a pressure of less than 10^{-4} mbar. It is one of the most challenging aspects in ICP-MS instrumentation. [16]

The vacuum interface is schematically shown in Figure 9. The coupling is accomplished by an intermediate vacuum region created by two interface cones, the sampler and the skimmer. Each of these cones, which can be made of nickel, copper or platinum, has a round hole with a diameter of less than 1 mm in its center. The hot plasma is transmitted through the sampler cone into an intermediate vacuum region with a pressure of about 1 mbar. After rapid expansion of the plasma jet, a fraction of the gas passes through the skimmer cone into a chamber with pressure of the mass spectrometer. [17]
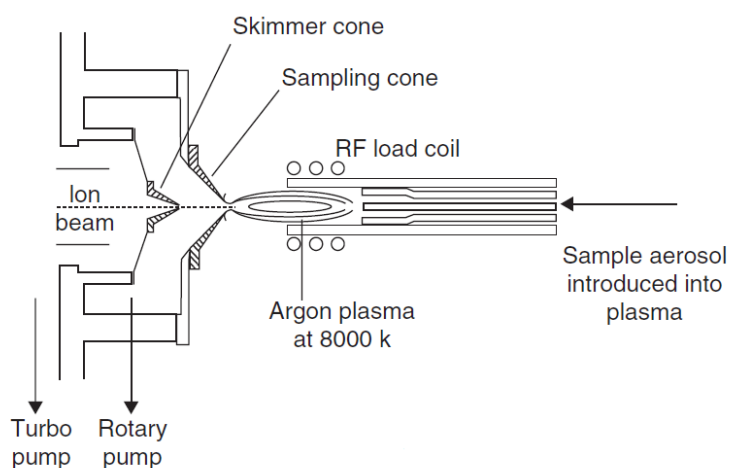

Figure 9: Typical vacuum interface used in ICP-MS instruments [17]

2.3.3   Ion optics

After transmission through the interface, ion optics separate the ions from electrons, photons and neutral atoms and focuses them into the mass analyzer. Because scattered ions will not be detected, the ion-focusing lenses are crucial for the overall sensitivity of the ICP-MS device. Focusing is achieved by the use of constant electric fields to deflect and accelerate the ions. [17]

The removal of neutral species and photons is also an important task of the ion optics, because they would otherwise be registered as additional ion counts by the detector. Therefore, in most ICP-MS devices used today the entrance of the mass analyzer is offset from the plasma axis and the ion beam is directed through a chicane, or the ion beam is deflected in a 90° angle. [23]

2.3.4   Quadrupole mass analyzer

Its compactness, cheapness, and ruggedness combined with its high scan rates make the quadrupole mass analyzer the most common type used in elemental mass spectrometry. Entire mass spectra can be obtained in less than 100 ms. [16] In a quadrupole mass analyzer, ions are separated according to their m/z ratios based on the stability of their trajectories in oscillating electric fields.

A schematic drawing of a quadrupole mass analyzer is shown in Figure 10. It consists of four parallel cylindrical rods that serve as electrodes. Each opposing rod pair is connected electrically. A DC voltage as well as a variable radio-frequency AC voltage are applied to each pair of rods, which causes the entering ions to oscillate. Depending on the voltages, only ions with a specific m/z ratio have stable trajectories and reach the detector; all other ions strike the rods and are converted to neutral atoms or molecules. By fast variation of the applied voltages different m/z values can be measured within a short time scale.
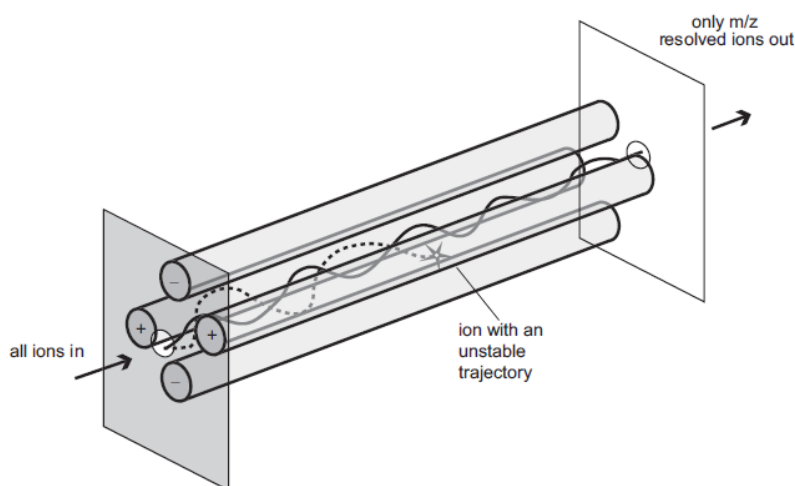

Figure 10: Schematic diagram of a quadrupole mass analyzer [23]

2.3.5   Channel electron multiplier (CEM)

Electron multipliers are the most commonly type of detectors used in mass spectrometry. A channel electron multiplier (CEM) is a special kind of electron multiplier with a continuous dynode shaped like a cornucopia.

The typical set-up of a channel electron multiplier is shown in Figure 11. It consists of a curved glass tube coated with a highly resistive material that generates electrons from ions hitting its surface. A high voltage of between -2600 and -3500 V is applied to the multiplier attracting cations into the funnel opening. The collision of an ion with the inner coating results in the ejection of one or more secondary electrons, which are attracted towards the grounded end of the tube and create more secondary electrons with each impact. An exponential cascade of electrons rapidly builds up, resulting in a large electron pulse and a multiplication of the signal by a factor of 10^7 to 10^8. [17]
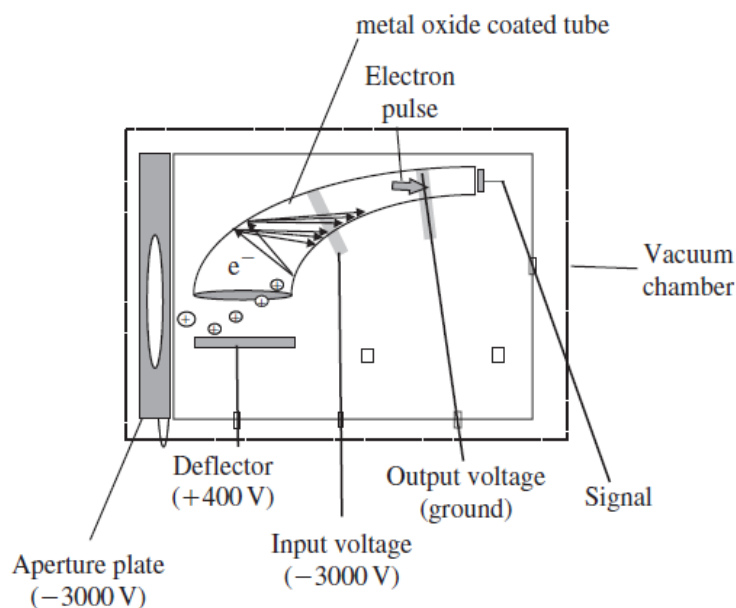
Figure 11: Schematic of a channel electron multiplier [17]

2.4 Laser ablation (LA) in chemical analysis

2.4.1 Principle and overview

Laser ablation (LA) is a technique for direct solid sampling widely used in analytical chemistry. In combination with ICP-OES or -MS it becomes a powerful method for direct elemental analysis, which features multi-element capability, great elemental coverage, low limits of detection (especially in the case of LA-ICP-MS), and a wide linear dynamic range. LA-ICP-OES and LA-ICP-MS also enable spatially resolved analysis including microanalysis, depth profiling analysis, and two-dimensional elemental mapping. Further advantages are the high sample throughput, minimal sample preparation, nearly non-destructiveness (< µg sample is required), the possibility of analyzing any type of solid material, and in the case of LA-ICP-MS even the access to isotopic information. [12]

The general set-up of a LA system is shown in Figure 12. A short-pulsed, high-power laser beam is focused onto a sample surface, which is placed in an ablation chamber. This leads to an ablation of a finite volume of the solid sample generating vapor, particles and agglomerates. The formed aerosol is transported into the ICP-OES (see section 2.2) or ICP-MS (see section 2.3) by a carrier gas flushed through the ablation chamber. Although sample introduction in ICP-OES and -MS is generally realized using Ar, the carrier gas through the ablation chamber is usually replaced by He due to a significant enhanced particle transport, resulting in increased sensitivity and sample material washout. [24]
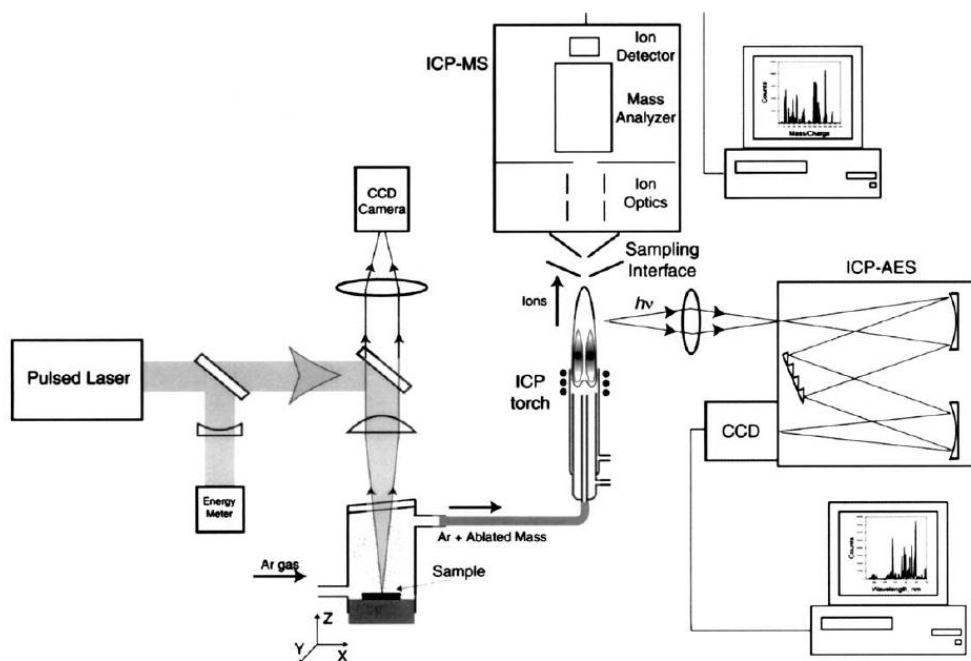
Figure 12: Schematic of a laser ablation system, using ICP-OES and/or ICP-MS for detection [12]

Ablation is affected by the wavelength and the pulse duration of the used laser. In general, lower wavelengths and shorter pulses improve the ablation behavior. Most lasers used to day utilize Nd:YAG ($Y_3Al_5O_{12}$) or excimer lasers with wavelengths in the low UV and pulse durations in the nanosecond range. Also highly expensive Ti:Sapphire femtosecond lasers with superior ablation properties are used. [22] The laser ablation system used in this work is equipped with a 213 nm Nd:YAG laser.

2.4.2   Nd:YAG laser

Solid-state Nd:YAG (neodymium-doped yttrium aluminium garnet; Nd:$Y_3Al_5O_{12}$) systems are widely used for laser ablation, since they are relatively inexpensive, require little maintenance, and are easily incorporated into several commercial laser ablation systems. The fundamental wavelength of Nd:YAG lasers is in the near-IR at 1064 nm. Wavelengths of 532, 355, 266 and 213 nm are achievable by optical frequency doubling, tripling, quadrupling, and quintupling. [12]

The lasing medium of a Nd:YAG laser is a doped yttrium aluminum garnet ($Y_3Al_5O_{12}$). The dopant, triple ionized Nd, replaces a small fraction of Y-ions and provides the lasing activity in the crystal. Figure 13 shows the four energy levels of Nd:YAG. By optical pumping using a flash tube, Nd-ions in the ground state are excited to the upper energy band E_2. From there, a non-radiative transition to the metastable energy level E_1 occurs immediately. Due to its relatively long lifetime, more and more electrons reach this metastable state, leading to a population inversion in which most of the ions are excited. A photon produced by a spontaneous transition triggers further emission of photons, which leads to a chain reaction and thereby to the generation of a laser beam. [25]

Nd:YAG lasers operate in pulsed mode as well as in continuous mode. Pulsed Nd:YAG lasers are typically operated in Q-switching mode: An optical switch inserted in the laser cavity is closed until a maximum population inversion is achieved. Thereby, very short and very high power pulses are produced. [25]
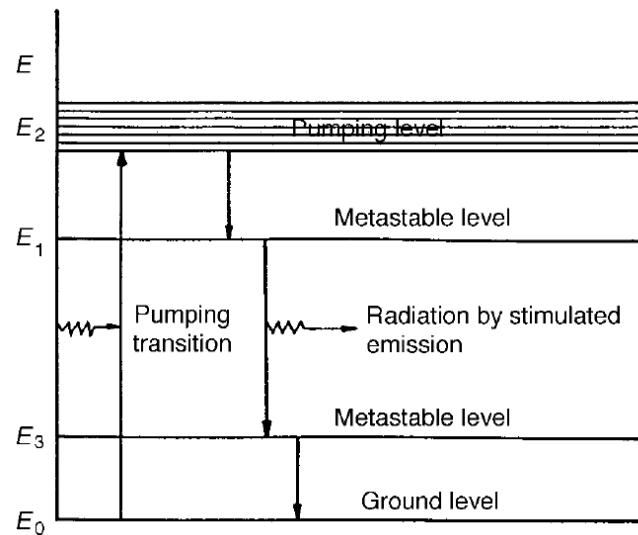

Figure 13: Energy level diagram of a Nd:YAG laser [25]

2.4.3   Signal quantification

Although the coupling of ICP-OES and -MS with laser ablation exhibits several great advantages in the analysis of solid samples, there is also one major drawback compared to liquid sampling experiments: While analyte quantification in liquid samples is easily achieved by external calibration employing (aqueous) standard solutions with known analyte concentration, quantification is a much harder task in laser ablation experiments.

The difficulty of LA-ICP-OES and LA-ICP-MS measurements is that the obtained signals are usually not entirely representative for the elemental composition of the investigated sample. The reasons for this are sample-dependent ablation behavior and elemental fractionation during the ablation process itself, the transport of the aerosol particles into the ICP as well as the vaporization, atomization, and ionization in the ICP. Therefore, calibration often requires standards being similar to the samples. Appropriate certified reference materials (CRMs) are available for some kinds of material, but do not cover every type of sample. Thus, the in-house preparation of matrix-matched standards is usually required for external calibration. [11, 12]

Signal normalization to an internal standard further improves the accuracy of the quantitative results, since variations in sample ablation and transport as well as changing plasma conditions can be corrected. However, this is only possible if the internal standard element is homogeneously distributed within the matrix and its concentration is known or at least equal in all standards and samples. [11]

Since many materials do not contain an internal standard with invariant concentration, it is often required to determine its content by an independent method prior to LA measurement. To circumvent this limitation, an alternative approach using all matrix elements for internal standardization by a summed-spectrum normalization can be used. [26]

To get accurate results, this total sum of signals normalization technique requires that all measured elements have almost the same sensitivity. For reasons already mentioned, this assumption is not accurate for many sample types. Among other improvements of this normalization method, Liu et al [13] presented an internal standard-independent calibration strategy for LA-ICP-MS analysis of anhydrous minerals and glasses. This technique is based on the consideration that the sum of all element concentrations expressed as oxides should be 100 wt% for a given anhydrous silicate. In this approach, Equation 1 and Equation 2 are used for the quantification of the measurement.

$$C^i_{sam} = \frac{100 \cdot cps^i_{sam} \cdot l^i}{\sum_{k=1}^{N} cps^k_{sam} \cdot l^k} \qquad \text{Equation 1}$$

$$l^i = \sum_{j=1}^{n} \left(\frac{C^i_{rm^j}}{cps^i_{rm^j}} \cdot \frac{C^i_{rm^j}}{\sum_{j=1}^{n} C^i_{rm^j}} \right) \qquad \text{Equation 2}$$

N…number of measured elements

n…number of reference materials used as external standard

C^i_{sam} …concentrations of analyte element i in the sample

$C^i_{rm^j}$…concentrations of analyte element i in the reference material j

cps^i_{sam} (cps^k_{sam}) …net count rate of element i (k) in the sample

$cps^i_{rm^j}$…net count rate of element i in the reference material j

3   Experimental

3.1   Chemicals and reagents

All chemicals used in this work are listed in Table 1. For the synthesis of $Li_{7-3x}Al_xLa_3Zr_2O_{12}$ reagents of synthesis grade or higher were used. All chemicals used throughout the analytical process were of p.a. grade or higher.

Table 1: List of used chemicals

		Assay	Supplier
Synthesis	Lithium carbonate	≥ 99%	Merck, Germany
	Aluminium(III) oxide	≥ 99.5%	Sigma-Aldrich, Germany
	Lanthanum(III) oxide	≥ 99.99%	Carl Roth, Germany
	Zirconium(IV) oxide	≥ 99%	Carl Roth, Germany
Analysis	Sodium tetraborate, anhydrous	≥ 98%	Merck, Germany
	Hydrochloric acid	65 vol%	Merck, Germany
	Hydrofluoric acid	40 vol%	Merck, Germany
	Nitric acid	37 vol%	Merck, Germany

The water used for all experiments was deionized via reverse osmosis and further purified with a Barnstead EASYPURE II system (Thermo Fisher Scientific, USA). Thereby, ultrapure water with a resistivity of 18.2 MΩ cm^{-1} was obtained.

Single element ICP-standard solutions were purchased from Merck, Germany. All used standard solutions are given in Table 2.

Table 2: List of used standard solutions

	Standard	Concentration [mg kg^{-1}]
Eu	Certipur® 170317	984 ± 5
Al	Certipur® 170301	985 ± 5
Ga	Certipur® 170319	985 ± 6
La	Certipur® 170327	988 ± 4
Li	Certipur® 170329	983 ± 5
Zr	Certipur® 170370	986 ± 4

3.2   LLZO synthesis

All syntheses were carried out at the department of Chemistry and Physics of Materials at the Paris Lodron University of Salzburg by Mag. Reinhard Wagner.

$Li_{7-3x}Al_xLa_3Zr_2O_{12}$ garnets with intended Al contents x = 0.00, 0.05, 0.10, 0.15, 0.20, 0.25, 0.30, 0.35, 0.40 were synthesized by a high-temperature sintering route based on the procedure described by Wagner et al. [27]

Li_2CO_3, Al_2O_3, La_2O_3, and ZrO_2 were used as starting materials. The reagents were weighted out in their intended stochiometric proportions with an excess of 10 wt% Li_2CO_3 to compensate LiO_2 loss during sintering. Carbonate and oxides were ground and mixed in an agate mortar under addition of isopropyl alcohol and then cold-pressed uniaxially. The resulting pellets were put into an alumina crucible and heated to 850 °C with a rate of 5 °C min^{-1} and calcinated for 4 h. To avoid undesired Al contamination from the crucible, the pellets were placed on a pellet of pure LLZO.

After cooling down, the pellets were ground in an agate mortar and ball-milled for 1 h under isopropyl alcohol (800 rpm, 2 mm ZrO_2 balls) using a Pulverisette 7 planetary mill (Fritsch, Germany). After drying, the powder was again cold-pressed and the resulting pellets again put into an alumina crucible. To avoid incorporation of Al^{3+} from the crucible as well as formation of extra phases due to Li loss during sintering, the samples pellets were placed between two pellets of pure LLZO. The final sintering step was carried out by heating the pellets in a muffle furnace with a rate of 5 °C min^{-1} and sintering for 6 h at 1230 °C.

3.3   Instrumental

3.3.1   ICP-OES

For ICP-OES measurements, an iCAP 6500 RAD (Thermo Fisher Scientific, USA) equipped with an echelle-type monochromator and a CID detector was used. Data acquisition was performed using Qtegra software provided by the manufacturer of the instrument.

Introduction of liquid samples was carried out using an ASX-520 autosampler (CETAC Technologies, USA). The autosampler was connected by PTFE tubing to a Thermo high solid sample introduction kid consisting of a quartz concentric nebulizer and a quartz cyclone spray chamber without ascension tube. The used plasma torch contained a quartz injector tube of 1.5 mm inner diameter.

The laser ablation system used for introduction of solid samples is described in section 3.3.3. For LA-experiments, a plasma torch with a corrosion-resistant ceramic injector tube of 1.5 mm inner diameter was used.

Detailed information about the analysis parameters of the ICP-OES instrumentation used for the analysis of digested samples and for LA-ICP-OES experiments are shown in Table 3.

Table 3: Instrumental parameters Thermo iCAP 6500 RAD

	Conventional ICP-OES		LA-ICP-OES	
RF power	1200 W		1200 W	
Radial observation height	12 mm		12 mm	
Plasma gas flow	12 l min^{-1}		12 l min^{-1}	
Nebulizer gas flow	0.6 l min^{-1}		-	
Auxiliary gas flow	0.8 l min^{-1}		0.5 l min^{-1}	
Integration time	5 s		10 s	
Replicates per sample	5		5	
Purge pump rate	1.6 ml min^{-1}		-	
Analysis pump rate	0.8 ml min^{-1}		-	
Analytical wavelengths				
Al	396.152 nm	-	396.152 nm	-
Eu	281.396 nm	381.967 nm	-	
Ga	294.364 nm	-	-	
La	333.749 nm	412.323 nm	261.034 nm	419.655 nm
Li	670.784 nm	-	610.362 nm	670.784 nm
Zr	339.198 nm	343.823 nm	257.139 nm	274.256 nm

3.3.2 ICP-MS

During this work an iCAP Qc quadrupole ICP-MS (Thermo Fisher Scientific, Germany) was used. Data acquisition was carried out using Qtegra software provided with the instrument. By coupling with a laser ablation system (see section 3.3.3), direct solid sample introduction was performed. Instrumental parameters used for all ICP-MS measurements are given in Table 4.

Table 4: Instrumental parameters Thermo iCAP Qc

	LA-ICP-MS
RF power	1550 W
Plasma gas flow	14 l min^{-1}
Auxiliary gas flow	0.8 l min^{-1}
Dwell time per isotope	10 ms
Cones	Ni
Measured isotopes	^{7}Li, ^{13}C, ^{27}Al, ^{71}Ga, ^{90}Zr, ^{93}Nb, ^{138}La, ^{181}Ta

Before every experiment the measurement parameters concerning the MS instrumentation were optimized using NIST 612 trace metals in glass standard (National Institute of Standards and Technologies, US) for maximum [115]In signal.

3.3.3   LA system

For LA experiments, a NWR213 laser ablation system (ESI, USA) equipped with a frequency quintupled 213 nm Nd:YAG laser and a fast-washout ablation cell was used. The coupling with either ICP-OES or -MS instrumentation was achieved using PTFE tubing (inner diameter 2 mm). For cell washout, He was used as carrier gas, which was mixed with Ar make-up gas upon introduction into the plasma.

Depending on the experiment different ablation methods and laser parameters were used. A detailed description of these methods and the corresponding laser settings will be given later (section 3.5 and 3.6). A summary of the optimized laser ablation parameters used for the experiments is shown in Table 5.

Table 5: Instrumental parameters New Wave 213

	LA-ICP-MS Imaging	LA-ICP-MS External calibration	LA-ICP-OES External calibration
Average fluence			
Pre-Ablation	1.89 J s^{-2}	3.91 J s^{-2}	2.28 J s^{-2}
Ablation	13.42 J s^{-2}	5.90 J s^{-2}	2.15 J s^{-2}
Laser diameter			
Pre-Ablation	250 µm	110 µm	200 µm
Ablation	60 µm	110 µm	200 µm
Scan speed			
Pre-Ablation	600 µm s^{-1}	100 µm s^{-1}	100 µm s^{-1}
Ablation	180 µm s^{-1}	40 µm s^{-1}	40 µm s^{-1}
Repetition Rate	20 Hz	20 Hz	20 Hz
Warm up time	10 s	10 s	10 s
Carrier gas flow (He)	0.6 l min^{-1}	0.6 l min^{-1}	0.6 l min^{-1}
Make-up gas flow (Ar)	0.8 l min^{-1}	0.8 l min^{-1}	0.8 l min^{-1}

3.4   Bulk analysis using ICP-OES

3.4.1   Sample digestion

To ensure homogeneity all samples on which bulk analysis was performed were crushed and ground in an agate mortar. 50 mg of each sample was transferred into a Pt crucible together with 0.8 g borax. The mixtures were put into a CWF 1300 chamber furnace (Carbolite, Germany) and heated to 1000 °C at a heating rate of 10 °C min^{-1}. After 5 h at 1000 °C, the samples were cooled down to room temperature with a rate of 10 °C min^{-1} and removed from the furnace.

The solidified fusions were dissolved by adding 4.0 ml 65 vol% HCl, 0.5 ml 40 vol% HF and 20 ml high purity water. To fasten the process, the crucibles were placed on a heating plate and heated to approximately 90 °C. Evaporated water was replaced every hour. After complete dissolution, the samples were transferred into 50 ml centrifuge tubes (Brand, Germany) and diluted with 1 vol% HNO_3 to an overall volume of 50 ml. To ensure a complete transfer of the analyte, the Pt crucibles were rinsed three times with 1 vol% HNO_3.

For each LLZO sample 1 to 3 replicate digestions were performed; eight digestions were carried out at the same time. To monitor contamination acquired during the process, a procedural blank without sample was performed in an additional ninth crucible.

A schematic drawing of the procedure used for sample digestion is shown in Figure 14.
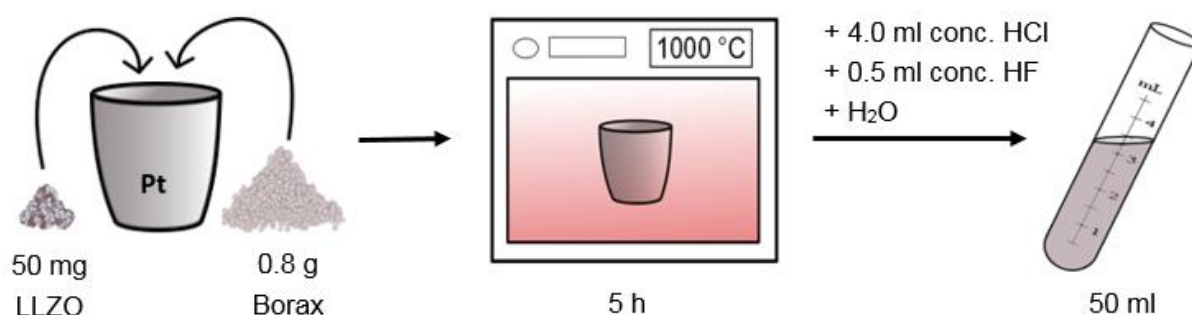
Figure 14: Flowchart of the borax fusion used for sample digestion

3.4.2   Measurement method

For ICP-OES measurement, 0.1 ml of each digestion mixture was transferred into a 12 ml polyethylene testing tube (VWR, Austria) and filled to a total volume of 10 ml using 1 vol% HNO_3. An Eu ICP-standard solution was added to a final concentration of 0.2 μg ml^{-1} serving as internal standard.

Aqueous calibration standards containing Al, Ga, La, Li, and Zr were used for signal quantification. For the preparation of these, elemental ratios were chosen according to the nominal chemical composition of the $Li_{7-3x}Al_xLa_3Zr_2O_{12}$ samples. Ga was included in the standards, because Ga contaminations have been found in preliminary experiments. Single

element ICP-standard solutions were used for the preparation of six multielement standards. The concentration ranges covered by these standards are shown in Table 6. To ensure that the matrix of the standards matches the sample matrix, an aqueous solution containing HNO_3, HCl, HF and borax in adjusted concentrations was used for dilution of the standards.

Table 6: Concentration ranges covered by the aqueous calibration standards used for ICP-OES measurements

Element	Concentration range [ng ml^{-1}]
Al	150 - 15
Ga	40 - 4
La	6000 - 600
Li	1000 - 100
Zr	3000 - 300

As rinse solution between consecutive ICP-OES sample measurements an aqueous solution containing 3 vol% HNO_3, 0.5 vol% HCl, and 0.05 vol% HF was utilized. For every element the two most sensitive and non-interfered emission lines were measured. Although only one line was used for quantification, the results of both were compared to exclude the possibility of spectral interferences. In case of Al and Ga only one emission line was useable. A summary of all used analytical wavelengths is given in Table 7.

Table 7: Analytical wavelengths used for ICP-OES measurements

Element	Emission line [nm]	Use	Normalization
Eu	281.394	Internal standard	-
	381.967	Internal standard	-
Al	396.152	Quantification	Eu 381
	-	-	-
Ga	294.364	Quantification	Eu 281
	-	-	-
La	412.323	Quantification	Eu 281
	333.749	Quality control	Eu 281
Li	670.784	Quantification	Eu 381
	-	Quality control	-
Zr	343.823	Quantification	Eu 281
	339.198	Quality control	Eu 281

All signals were normalized to an Eu signal to correct instrumental drifts and differences in matrix composition. Depending on which wavelength provides the better correction, the Eu 281.394 or the Eu 381.967 emission line was used.

Because the impact of instrumental drifts can vary in different spectral regions and the wavelengths of the Eu emission lines do not match the ones of the analytes perfectly (especially in case of Li), instrumental drift not corrected by normalization to the internal standard can occur. To monitor this effect as well as to improve the stability of the method against it, the calibration standards were measured not consecutively but separately between the samples (every 3 - 4 samples 1 standard) and in random order. For further quality assurance and further improvement of the analytical accuracy, every sample was measured three times using different calibrations. A typical sample list using this method is given in Table 8. Because no significant differences between the three measurements have been observed, the results of each sample were averaged.

Table 8: Example of a sample list for the threefold ICP-OES analysis of 15 samples (5 LLZO garnets, 3 digestion replicates each) using three different calibrations. Standards measured between the samples in random order for better compensation of instrumental drifts.

Sample Nr.	Sample		Sample Nr.	Sample		Sample Nr.	Sample
1	Standard 4		22	Standard 4		43	Standard 4
2	LLZO 1 Digestion 1		23	LLZO 1 Digestion 1		44	LLZO 1 Digestion 1
3	LLZO 2 Digestion 1		24	LLZO 2 Digestion 1		45	LLZO 2 Digestion 1
4	LLZO 3 Digestion 1		25	LLZO 3 Digestion 1		46	LLZO 3 Digestion 1
5	Standard 1		26	Standard 1		47	Standard 1
6	LLZO 4 Digestion 1		27	LLZO 4 Digestion 1		48	LLZO 4 Digestion 1
7	LLZO 5 Digestion 1		28	LLZO 5 Digestion 1		49	LLZO 5 Digestion 1
8	LLZO 1 Digestion 2		29	LLZO 1 Digestion 2		50	LLZO 1 Digestion 2
9	Standard 6		30	Standard 6		51	Standard 6
10	LLZO 2 Digestion 2		31	LLZO 2 Digestion 2		52	LLZO 2 Digestion 2
11	LLZO 3 Digestion 2		32	LLZO 3 Digestion 2		53	LLZO 3 Digestion 2
12	LLZO 4 Digestion 2		33	LLZO 4 Digestion 2		54	LLZO 4 Digestion 2
13	Standard 2		34	Standard 2		55	Standard 2
14	LLZO 5 Digestion 2		35	LLZO 5 Digestion 2		56	LLZO 5 Digestion 2
15	LLZO 1 Digestion 3		36	LLZO 1 Digestion 3		57	LLZO 1 Digestion 3
16	LLZO 2 Digestion 3		37	LLZO 2 Digestion 3		58	LLZO 2 Digestion 3
17	Standard 3		38	Standard 3		59	Standard 3
18	LLZO 3 Digestion 3		39	LLZO 3 Digestion 3		60	LLZO 3 Digestion 3
19	LLZO 4 Digestion 3		40	LLZO 4 Digestion 3		61	LLZO 4 Digestion 3
20	LLZO 5 Digestion 3		41	LLZO 5 Digestion 3		62	LLZO 5 Digestion 3
21	Standard 5		42	Standard 5		63	Standard 5

Calibration 1 (rows 1–21), Calibration 2 (rows 22–42), Calibration 3 (rows 43–63)

3.5   Imaging experiments using LA-ICP-MS

Two-dimensional distribution images of various LLZO samples were created using LA-ICP-MS. The surfaces as well as the cross-sections of whole pellets were analyzed. To expose the cross-section of a pellet, it was cut in half using a rotary tool (Dremel 8200, Germany) and ground down using 200 mm SiC Foil (P500, 200 mm dia, Struers, Denmark).

Sample ablation was carried out using line scan patterns with adjoining lines, which is visualized in Figure 15. A laser beam diameter of 60 µm and a scan speed of 180 µm s^{-1} were used for all documented imaging experiments.

A pre-ablation step consisting of a similar line scan pattern with a laser beam diameter of 250 µm was installed prior to the distribution measurements. The pre-ablation was performed to avoid surface contamination as well as to remove an approximately 10 nm thick Li_2CO_3 layer that forms as a result of LLZO exposure to air. [28]
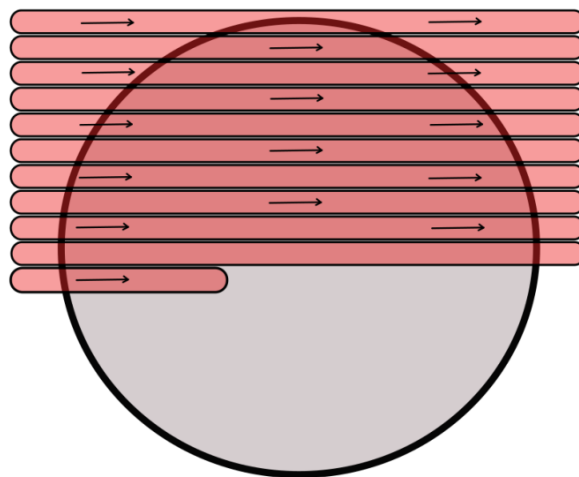
Figure 15: Line scan pattern used for creation of distribution images by LA-ICP-MS

Elemental distribution Images were created from the recorded time resolved intensities for the measured isotopes using the software ImageLab (v.1.90, Epina GmbH, Austria). To compensate differences in material ablation and instrumental drifts during measurement time, all recorded signals were normalized to the intensity of the isotope ^{138}La.

3.6   Quantification of LA experiments

3.6.1   Preparation of matrix-matched standards

For the preparation of matrix-matched standards, homogenous LLZO powders with different Al content ("$Li_{7-3x}Al_xLa_3Zr_2O_{12}$") were pressed into pellets. About 1 g of each sample was transferred into a flexible silicone rubber mold and was cold pressed using a mechanical isostatical press (Paul-Otto Weber, Germany). The procedure was carried out using a pressure of 300 MPa. The used mold and a LLZO sample in pressed form are shown in Figure 16.
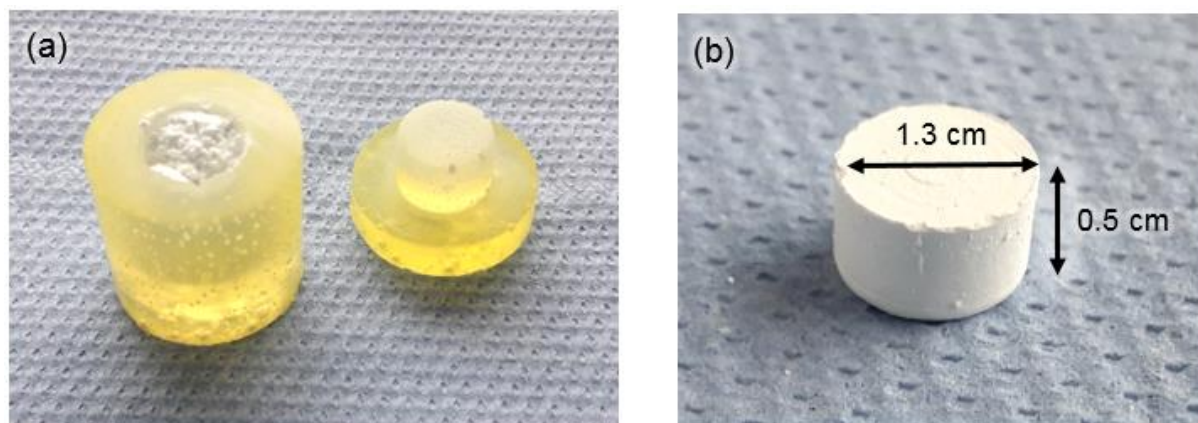
Figure 16: Images of (a) flexible mold used for isostatic pressing and (b) pressed LLZO-sample

3.6.2   External calibration

Since the pressed pellets used as calibration standards consist of individual grains with different chemical composition, it is necessary to ablate enough sample to make sure that the ablated material is representative for the whole pellet. To achieve that, multiple line scan patterns and larger laser beam diameters were used for the LA measurement of the calibration standards. Per sample four line scan patterns were applied and each pattern was ablated three times. Figure 17 shows a graphical representation of this ablation method. Laser beam diameters of 110 µm (LA-ICP-MS) or 200 µm (LA-ICP-OES) were used.

Laser energy, repetition rate and scan speed were optimized to yield controlled ablation behavior (i.e., defined spots of material ablation) with signals as stable as possible (i.e., temporal relative deviation of the raw signals). A laser beam with an average fluence of 2.15 J cm^{-2}, a repetition rate of 20 Hz and a scan speed of 120 µm s^{-1} was used for all documented experiments.

To avoid surface contamination, a pre-ablation step using similar line scan patterns and laser settings was carried out. In contrast to the actual measurement, each line scan pattern was ablated just once.
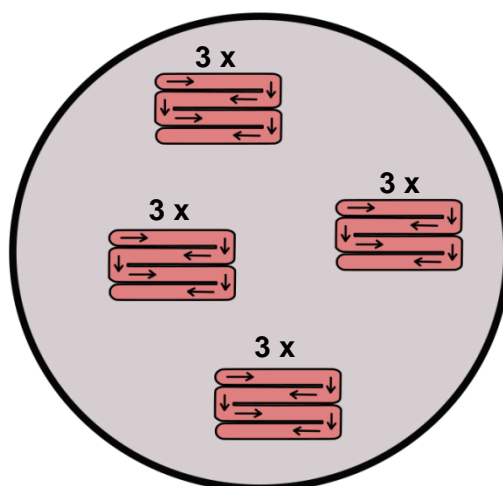
Figure 17: Line scan pattern used for the LA measurement of the pressed LLZO standards. Each pattern was ablated three times

All isotopes measured by LA-ICP-MS as well as all analytical wavelengths used for LA-ICP-OES measurement are summarized in Table 9.

Table 9: Analyzed isotopes and emission lines used for external calibration of LA-ICP-MS and LA-ICP-OES measurements, respectively.

Element	LA-ICP-MS	LA-ICP-OES	
	Isotope	Emission line [nm]	Use
Al	^{27}Al	396.152	Quantification
		-	-
La	^{138}La	261.034	Quantification
		419.655	Quality control
Li	^{7}Li	610.362	Quantification
		670.784	Quality control
Zr	^{90}Zr	274.256	Quantification
		257.139	Quality control

For the correction of variations in sample ablation and transport as well as instrumental drifts, signal normalization is necessary. Two different normalization approaches were used: On the one hand, all signals were normalized to the intensity of the La signal assuming that La is distributed in all samples equally. On the other hand, the internal standard-independent normalization technique presented by Liu et al [13] was applied (see Equations 1+2). Therefore, the concentrations of the measured elements were expressed as the corresponding oxides (Al_2O_3, Li_2O, La_2O_3, ZrO_2) and normalized to 100 wt%.

3.6.3   Sample measurement

For the LA analysis of various LLZO pellets, the prepared matrix-matched standards were used for external calibration. To minimize effects of instrumental drifts and to ensure plasma conditions and ablation behavior as similar as possible, all samples were analyzed directly after the standards using the same instrumental parameters and laser settings. Only the scan speed was reduced to 25 µm s^{-1} to obtain better spatial resolution. To make sure that this has no effect on the ablation behavior, experiments with different scan speeds were carried out in advance.

The ablation method used for the analysis of the samples is shown in Figure 18. Single line scans across the whole LLZO pellets were carried out. To obtain lateral resolution, each line scan was divided into 10 s regions for data acquisition, which results in about twenty regions per sample. Each region was quantified individually using the external calibration received by the measurement of the prepared matrix-matched LLZO standards.
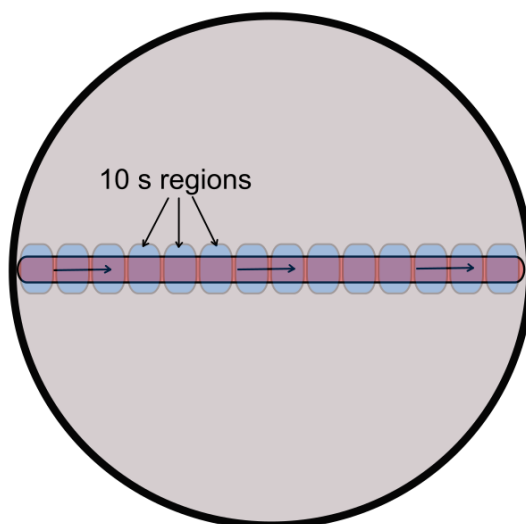
Figure 18: Ablation pattern used for the quantitative spatially resolved analysis of LLZO pellets. For data acquisition, the line scan was divided into 10 s regions and each region quantified individually.

4 Results and discussion

4.1 Bulk analysis of LLZO samples

4.1.1 Process control of a "$Li_{6.4}Al_{0.2}La_3Zr_2O_{12}$" synthesis

Starting materials, intermediates and product of a "$Li_{6.4}Al_{0.2}La_3Zr_2O_{12}$" synthesis were analyzed to investigate possible changes of the chemical composition during the different synthesis steps. The bulk analysis was carried out using ICP-OES measurement in combination with a borax fusion for sample digestion.

To improve the accuracy of the used method, each LLZO sample was digested three times. The obtained values for these replicate digestions were averaged and the corresponding standard deviations were calculated. The final results of the analysis are summarized in Table 10.

Table 10: Chemical composition of the starting materials, intermediates and the product of a LLZO garnet with the intended chemical composition $Li_{6.4}Al_{0.2}La_3Zr_2O_{12}$. The stated measurement uncertainties correspond to the standard deviations derived from the measurement of three replicate digestions.

	Sample	Starting materials	Calcinated
	Al	0.56 ± 0.01	0.67 ± 0.04
	Ga	0.17 ± 0.02	0.18 ± 0.01
wt%	La	41.7 ± 1.5	47.1 ± 1.7
	Li	4.92 ± 0.08	5.46 ± 0.15
	Zr	17.6 ± 0.5	20.3 ± 0.6
	Other	35.1 ± 2.0	26.3 ± 2.5
	Al/La	0.069 ± 0.002	0.074 ± 0.003
Atomic ratios	Ga/La	0.008 ± 0.001	0.008 ± 0.000
	Li/La	2.37 ± 0.05	2.32 ± 0.04
	Zr/La	0.64 ± 0.01	0.66 ± 0.01
	Formula[1]	$Li_{7.10}Al_{0.21}Ga_{0.02}La_3Zr_{1.93}O_{12.3}$	$Li_{6.97}Al_{0.22}Ga_{0.02}La_3Zr_{1.97}O_{12.3}$

	Sample	Calcinated + milled	Sintered
	Al	0.57 ± 0.01	0.67 ± 0.01
	Ga	0.16 ± 0.01	0.16 ± 0.01
wt%	La	39.9 ± 0.6	47.4 ± 1.2
	Li	4.71 ± 0.03	5.11 ± 0.03
	Zr	17.4 ± 0.1	20.7 ± 0.5
	Other	37.3 ± 0.8	25.9 ± 1.7
	Al/La	0.073 ± 0.001	0.073 ± 0.002
Atomic ratios	Ga/La	0.008 ± 0.001	0.008 ± 0.001
	Li/La	2.36 ± 0.02	2.16 ± 0.05
	Zr/La	0.66 ± 0.01	0.67 ± 0.00
	Formula[1]	$Li_{7.08}Al_{0.22}Ga_{0.02}La_3Zr_{1.99}O_{12.4}$	$Li_{6.47}Al_{0.22}Ga_{0.02}La_3Zr_{2.00}O_{12.1}$

[1] Calculated, based on atomic ratios. O contents are estimated from charge balance considerations.

The mass fractions of Al, Ga, La, Li, and Zr were calculated based on the original sample mass used for the digestion. The mass fraction, which could not be attributed to any of these elements, was summarized in the category "other" (e.g., C, O). Furthermore, the empirical formula of each sample was calculated using the atomic ratios of the elements. 3 pfu (per formula unit) La were chosen as the fixed-point, because this is the expected value for La, which should not be affected by sintering process. The O contents are estimated from charge balance considerations.

Evaluated vs. anticipated chemical composition of the starting materials

Since the powder used as starting material is just a mixture of known amounts of different oxides and carbonates, the theoretical mass fraction of each element can be calculated easily. By comparison of these expected values with the measured ones, the accuracy of the ICP-OES measurement including sample digestion can be estimated. The relative deviations of measured mass fractions from the calculated ones as well as the relative standard deviations (RSDs) derived from the analysis of replicate digestions are visualized in Figure 19.
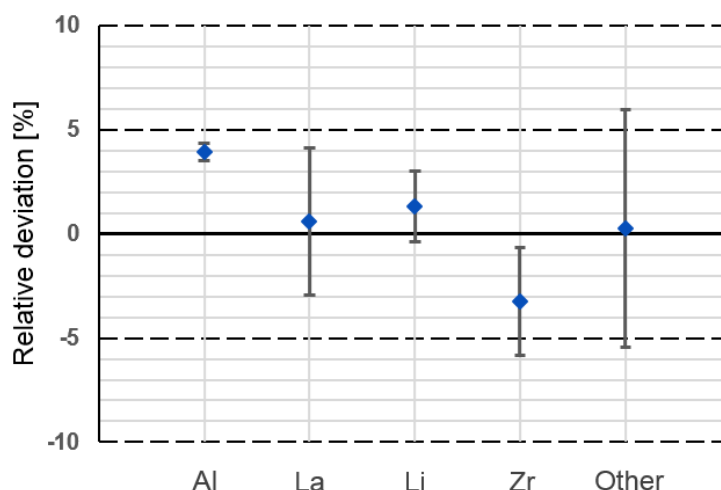
Figure 19: Relative deviations of the mass fractions measured by ICP-OES from expected values for the mixture of starting materials. The error bars represent the RSDs derived from the measurement of replicate digestions.

The RSDs are less than 4% for all measured elements: RSD(Al) = 0.9%, RSD(La) = 3.6%, RSD(Li) = 1.7%, and RSD(Zr) = 2.6%. The value for the category "other" is greater than that (RSD(other) = 5.5%), which can be explained by the fact that the mass fractions of all measured analytes are included into its calculation, leading to a greater uncertainty of measurement.

The relative deviation of the measured mass fractions from the theoretical values is less than 5% for all elements. In case of La, Li and the category "other" it is even less than 1.5%, which corresponds to an excellent consistency of evaluated and anticipated values. The remaining differences can be explained by measurement uncertainties, since the RSDs are greater than the corresponding relative deviation in all three cases.

The determined mass fraction of Al is 3.9% greater than excepted. Since contaminations during sample preparation can be excluded due to the analysis of procedural blanks, the most reasonable explanation of this small deviation is an Al contamination of one or more starting materials. Because the used amount of Li_2CO_3, ZrO_2, and La_2O_3 is by a factor 10 to 100 greater than the used amount of Al_2O_3, even small impurities can have a big effect. For example, an Al content of 0.1 wt% in the La_2O_3 powder increases the Al mass percentage of the resulting mixture by about 0.05%, which corresponds to a relative increase of the Al content by 9%.

The relative deviation of the Zr mass fraction is -3.3%, which means that less Zr than expected was measured. A possible reason for this small but significant deviation is that ZrO_2 was not digested completely. Since ZrO_2 is converted to easier digestible $Li_{6.4}Al_{0.2}La_3Zr_2O_{12}$ during synthesis, this incomplete digestion should not occur after sintering. The increased Zr ratio of the sintered LLZO compared to the starting materials (see Table 10) confirms this theory.

In addition to the expected elements, also a significant amount of Ga (0.17 ± 0.02 wt%) was detected. As already mentioned in the discussion of the determined Al mass fraction, contaminations during sample preparation can be excluded. Since spectral interferences can also be excluded due to the quality assurance measures described in the experimental section, contaminations of the starting materials are the most reliable explanation also in the case of Ga.

Except for Zr, the obtained results prove that no significant analyte loss occurred during sample digestion. As mentioned before, a loss of Zr was observable for ZrO_2, but not for sintered LLZO garnet. Therefore, the experiments prove that the used borax fusion in combination with the used ICP-OES measurement is a reliable method for the analysis of LLZO garnets.

Changes of the mass fractions during the synthesis

To visualize the changes of the chemical composition, the mass fractions of each element for every step of the LLZO synthesis are illustrated in Figure 20. It is evident that the mass fraction of "other" changes drastically, leading to changes in the mass fractions of the measured elements as well.

Included in the category "other" are all elements not measured, most notably O, C, and H in form of O^{2-} and CO_3^{2-} and H_2O. At first, the mass fraction of these elements decreases from 35.1 to 26.3% as a result of the calcination of the starting materials. Since Li_2CO_3 was used as starting a material, this can be explained by the loss of CO_2 due to the high temperature. Assuming that all starting materials are pure, the complete loss of CO_2 would result in an O mass fraction of 23.2%, which is less than the measured value and thus indicates that some CO_2 remains in the sample.

After milling of the calcinated sample, the mass fraction of the elements not measured is again increased to 37.3%. Although the actual reason for this increase is unclear, the most reasonable explanations are that the sample has absorbed H_2O or incorporated CO_2 again. The "other" mass fraction is decreased to 25.9% after the sintering, which shows that the H_2O and/or CO_2 is lost again during the high-temperature treatment.
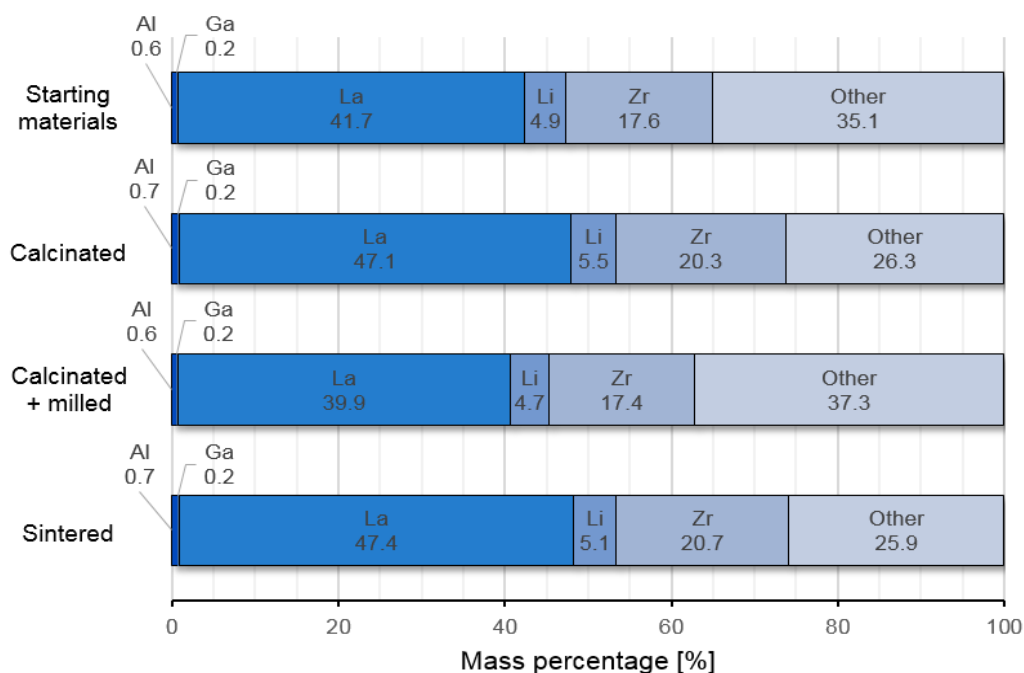
Figure 20: Elemental mass fractions of each step of a "$Li_{6.4}Al_{0.2}La_3Zr_2O_{12}$" synthesis

Because the described fluctuations also change the mass fractions of the measured elements, it is difficult to judge changes of these elements only by their mass fractions. For this purpose the comparison of the corresponding atomic ratios is more suitable.

Changes of the atomic ratios during the synthesis

To reveal changes of the Al, Ga, Li, La, and Zr content during the synthesis of the LLZO garnet, the atomic ratios after each synthesis step are visualized in Figure 21. Because La should not be affected by the synthesis, all other elements were set in relation to it. Changes of the La content are unlikely to occur because the high-temperature stability of La_2O_3 (boiling point ~ 4200 °C) prohibits La loss during sintering, and even small La contamination would not change the already high La content significantly.

The greatest changes are observable for the Li/La ratio. After sintering, the Li content is decreased by 8.9 ± 3.0% compared to the starting materials, which can be explained by the expected Li_2O loss during the high-temperature treatment. To compensate this loss of Li, an excess of the same percentage Li_2CO_3 should be used for the synthesis of LLZO garnets.

Although the mean values of the measurements also indicate a small Li loss of about 2% during the prior calcination step, this difference is not significant due to the fact that the RSD of the Li-determination is also in this range.
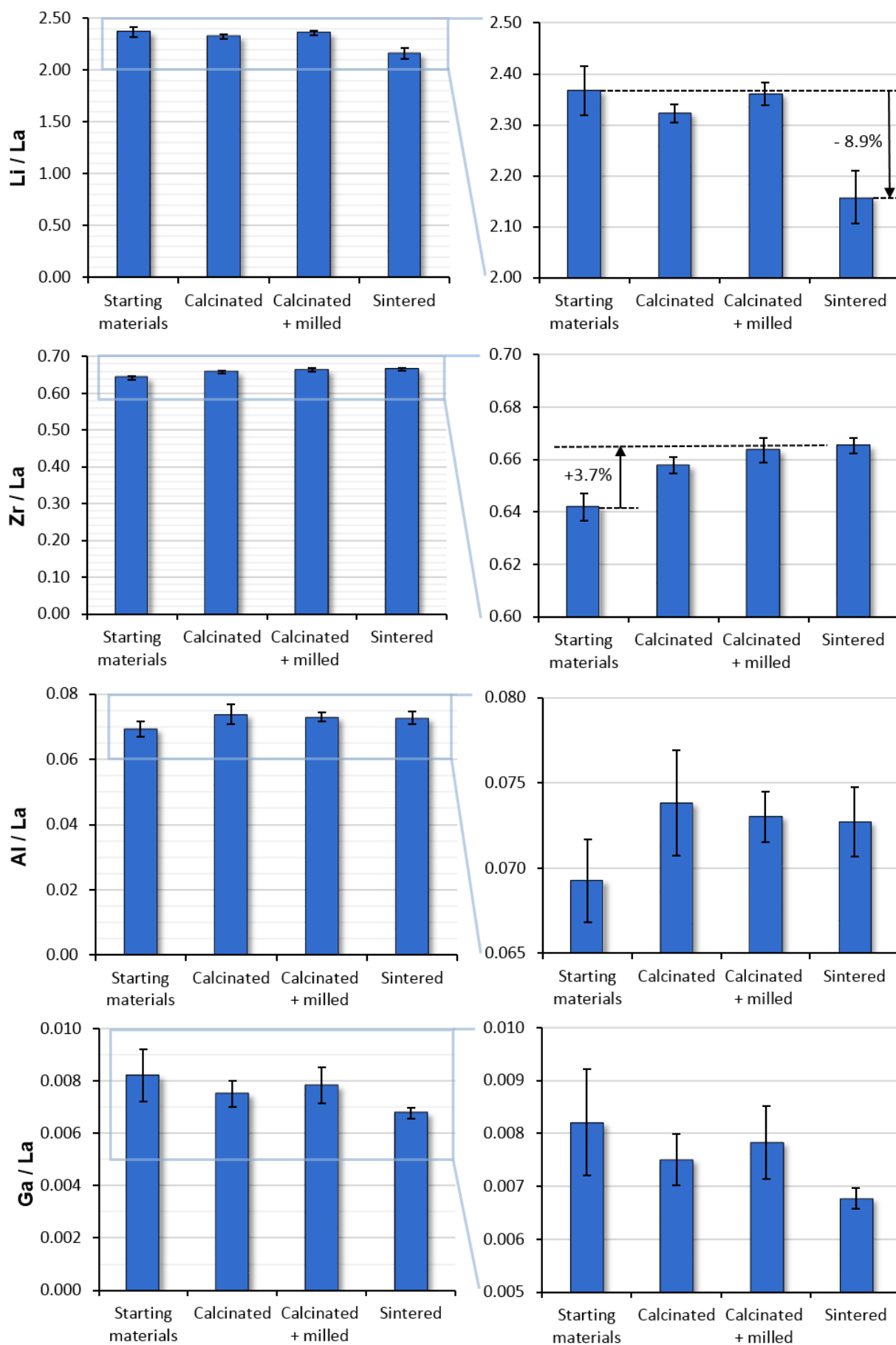
Figure 21: Atomic ratios of each step of a "$Li_{6.4}Al_{0.2}La_3Zr_2O_{12}$" synthesis. The error bars represent the RSDs derived from the measurement of replicate digestions.

Also a small increase of the Zr/La ratio by 3.7 ± 0.9 can be observed. This is probably not a result of actual changes of the Zr content during the synthesis, but of incomplete ZrO_2 digestion, as already described.

Furthermore, the results indicate a small increase of the Al content due to the calcination of the samples. Because the difference is in the same region as the RSD of the Al-analysis, no exact values can be given. An explanation for this increase would be Al contamination from the crucible. For the Ga/La ratio, no significant change is observable.

4.1.2 $Li_{7-3x}Al_xLa_3Zr_2O_{12}$ with varying Al content

A series of $Li_{7-3x}Al_xLa_3Zr_2O_{12}$ garnets with intended Al contents x = 0.00 - 0.40 were synthesized. To determine how well the intended and the actual chemical composition of the LLZO samples match, the garnets were characterized using ICP-OES. Since these samples were also used as standards for external calibration of LA measurements (see section 4.3), their chemical composition was also required for further experiments.

The determined chemical compositions are summarized in Table 11. As for the results shown in the previous section, the mass fractions of the elements are calculated based on the original sample mass used for the digestion.

Since only the sample with an intended chemical composition of $Li_{6.4}Al_{0.2}La_3Zr_2O_{12}$ ("Al 0.20") was digested multiple times, only in that case the standard deviation of the measurement could be determined based on the values of the replicate digestions. For all other samples the standard deviations of each element were calculated using the average RSDs of the measurements described in previous section.

Since the digestions of the "Al 0.20" sample were analyzed for the second time (the results of the first analysis are shown in section 4.1), the chemical compositions determined by the different measurements can be compared. No significant differences between the received mass fractions are observable, which indicates an excellent repeatability of the measurement method.

Table 11: Chemical composition of $Li_{7-3x}Al_xLa_3Zr_2O_{12}$ garnets with intended Al contents x = 0.00 - 0.40

Sample		"Al 0.00"	"Al 0.05"	"Al 0.10"
wt%	Al	0.38 ± 0.01	0.29 ± 0.01	0.41 ± 0.01
	Ga	0.20 ± 0.01	0.16 ± 0.01	0.13 ± 0.01
	La	49.7 ± 1.4	49.1 ± 1.4	48.7 ± 1.3
	Li	5.39 ± 0.08	5.47 ± 0.08	5.31 ± 0.07
	Zr	20.8 ± 0.5	21.0 ± 0.5	20.8 ± 0.5
	Other	23.5 ± 1.4	24.0 ± 1.4	24.7 ± 1.5
Atomic ratios	Al/La	0.040 ± 0.001	0.030 ± 0.001	0.043 ± 0.001
	Ga/La	0.008 ± 0.001	0.006 ± 0.001	0.005 ± 0.001
	Li/La	2.17 ± 0.03	2.23 ± 0.03	2.18 ± 0.03
	Zr/La	0.64 ± 0.01	0.65 ± 0.01	0.65 ± 0.01
Formula[1]		$Li_{6.51}Al_{0.12}Ga_{0.02}La_3Zr_{1.91}O_{11.8}$	$Li_{6.69}Al_{0.09}Ga_{0.02}La_3Zr_{1.95}O_{11.9}$	$Li_{6.55}Al_{0.13}Ga_{0.02}La_3Zr_{1.95}O_{11.9}$

Sample		"Al 0.15"	"Al 0.20"	"Al 0.25"
wt%	Al	0.55 ± 0.01	0.67 ± 0.01	0.81 ± 0.01
	Ga	0.15 ± 0.01	0.15 ± 0.04	0.15 ± 0.01
	La	48.1 ± 1.3	47.7 ± 0.6	48.5 ± 1.3
	Li	5.23 ± 0.07	5.11 ± 0.01	5.08 ± 0.07
	Zr	20.7 ± 0.5	20.4 ± 0.2	20.7 ± 0.5
	Other	25.3 ± 1.5	26.0 ± 0.8	24.7 ± 1.5
Atomic ratios	Al/La	0.059 ± 0.002	0.073 ± 0.001	0.086 ± 0.003
	Ga/La	0.006 ± 0.001	0.006 ± 0.002	0.006 ± 0.001
	Li/La	2.17 ± 0.03	2.15 ± 0.03	2.10 ± 0.03
	Zr/La	0.65 ± 0.01	0.65 ± 0.01	0.65 ± 0.01
Formula[1]		$Li_{6.52}Al_{0.18}Ga_{0.02}La_3Zr_{1.96}O_{12.0}$	$Li_{6.44}Al_{0.22}Ga_{0.02}La_3Zr_{1.96}O_{12.0}$	$Li_{6.29}Al_{0.26}Ga_{0.02}La_3Zr_{1.95}O_{12.0}$

Sample		"Al 0.30"	"Al 0.35"	"Al 0.40"
wt%	Al	0.93 ± 0.02	1.05 ± 0.02	1.19 ± 0.02
	Ga	0.13 ± 0.01	0.12 ± 0.01	0.13 ± 0.01
	La	48.7 ± 1.3	48.2 ± 1.3	46.9 ± 1.3
	Li	5.01 ± 0.07	4.87 ± 0.07	4.69 ± 0.07
	Zr	20.7 ± 0.5	20.7 ± 0.5	20.2 ± 0.4
	Other	24.6 ± 1.5	25.1 ± 1.5	26.9 ± 1.6
Atomic ratios	Al/La	0.099 ± 0.003	0.112 ± 0.004	0.130 ± 0.004
	Ga/La	0.005 ± 0.001	0.005 ± 0.001	0.005 ± 0.001
	Li/La	2.06 ± 0.03	2.02 ± 0.03	2.00 ± 0.03
	Zr/La	0.65 ± 0.01	0.65 ± 0.01	0.65 ± 0.01
Formula[1]		$Li_{6.19}Al_{0.30}Ga_{0.02}La_3Zr_{1.94}O_{11.9}$	$Li_{6.07}Al_{0.34}Ga_{0.02}La_3Zr_{1.96}O_{12.0}$	$Li_{6.00}Al_{0.39}Ga_{0.02}La_3Zr_{1.96}O_{12.0}$

[1] Calculated, based on atomic ratios. O contents are estimated from charge balance considerations.

Evaluated vs. intended chemical composition of the LLZO garnets

To determine to which extent the synthesized LLZO samples possess the desired chemical composition, the intended atomic ratios were calculated and compared to the measured ones. For the visualization of the differences, the corresponding deviations were plotted for each sample. The relative deviations of the Li/La and Zr/La atomic ratios from the intended values are shown in Figure 22.

The greatest difference of the Li/La ratio can be observed for the "Al 0.00" sample with a relative deviation of $7.0 \pm 1.5\%$. The relative deviations of all other samples are less than 5%. For the samples with an intended Al content of 0.15, 0.20, and 0.25 no significant difference between the desired and the measured value can be observed. This indicates that the right amount of Li_2CO_3 excess (10 wt%, see section 3.2) was used for the synthesis of these samples.

Furthermore, a trend of the relative deviation of the Li/La atomic ratio is observable. While for samples with a lower Al content the values are less than desired, the Al-rich samples show an increased Li/La ratio. This indicates that less Li was lost during the synthesis of the samples with a greater Al content. Therefore, the amount of LiO_2 loss during sintering seems to be dependent of the Al content, which means that the corresponding value determined in section 4.1.1 is only valid for LLZO samples with an intended chemical composition of $Li_{6.4}Al_{0.2}La_3Zr_2O_{12}$.
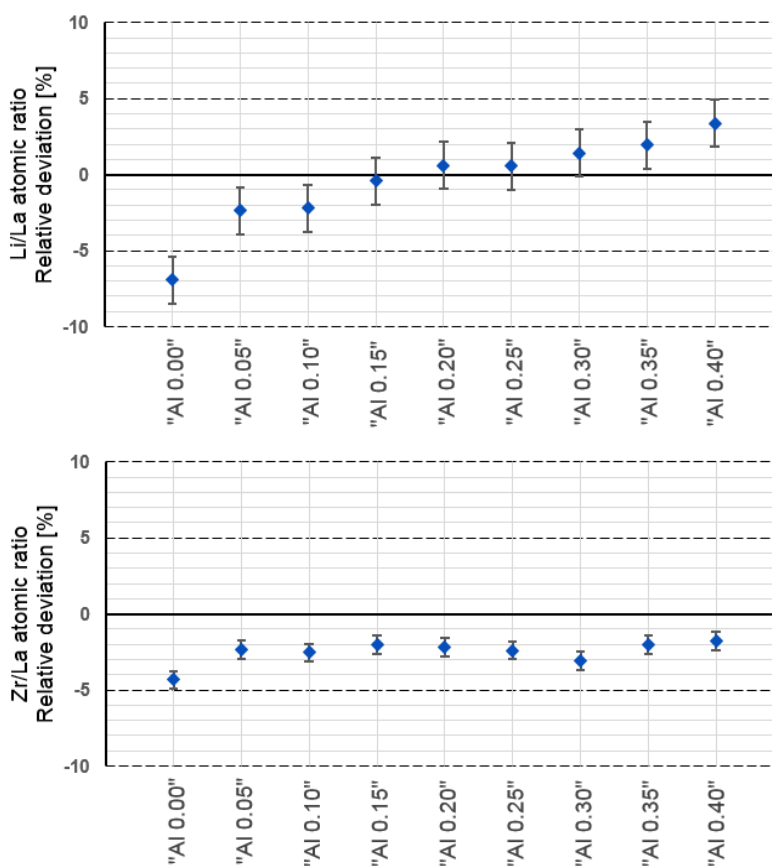
Figure 22: Relative deviations of the measured Li/La and Zr/La atomic ratios from the intended values for LLZO samples with different Al content. The error bars represent the average RSD of the analysis derived from the measurements of replicate digestions.

The measured Zr/La atomic ratio was less than intended for all samples. With -4.3 ± 0.6% relative deviation the greatest difference can be observed for the "Al 0.00" sample. All other samples show an almost equal Zr/La atomic ratio with a relative deviation to the intended value in the range of 1.7 to 3.0%. Possible reasons for these small but significant deviations are inaccuracies during the preparation of the calibration standards.

Since the intended Al and Ga contents are zero or close to it, the stating of absolute deviations is more suited to show the differences between the measured and desired values. The corresponding diagrams are displayed in Figure 23.
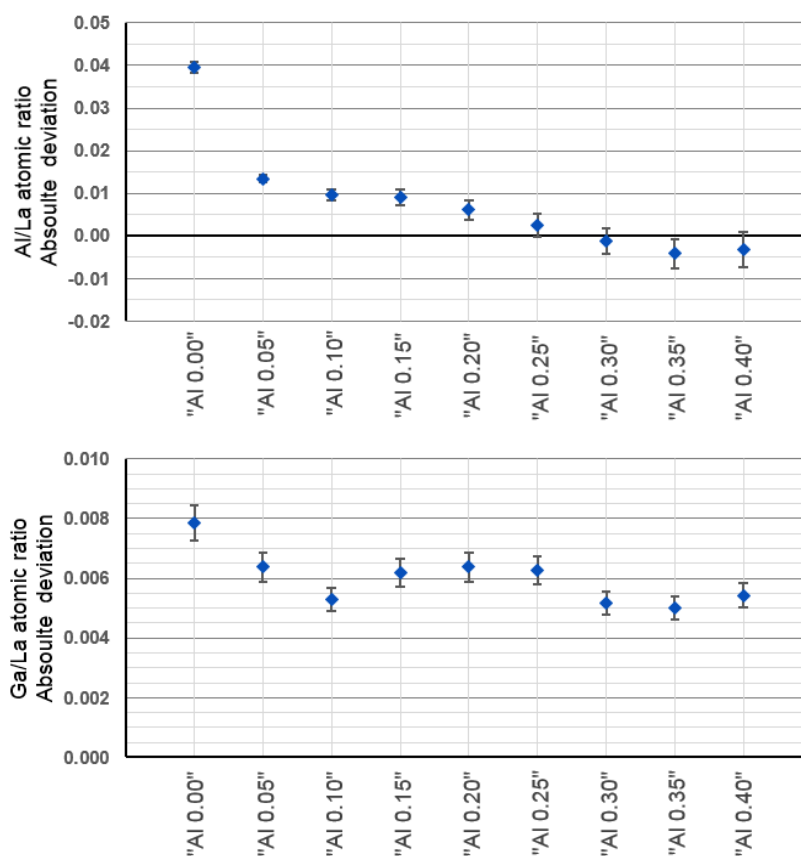
Figure 23: Absolute deviations of the measured Al/La and Ga/La atomic ratios from the intended values for LLZO samples with different Al content. The error bars represent the average RSD of the analysis derived from the measurements of replicate digestions.

Although the sample with an intended chemical composition of $Li_7La_3Zr_2O_{12}$ (pure LLZO) should be Al-free, an Al/La ratio of 0.040 ± 0.001 was measured. With greater Al content the differences are reduced, until no significant difference is observable for the four samples with the greatest Al contents. As for the Li/La ratio, a trend of the deviations can be observed, but in the opposite direction.

Since the absolute differences between measured and intended Al contents vary greatly, impure starting materials can be excluded as a reason for the Al contaminations. The results rather indicate that Al is incorporated during the sintering, but only in LLZO samples with a low

Al content. This could be related to the fact that Al-substitution stabilizes the cubic modification of LLZO. [14]

The measured Ga/La atomic ratios vary in the range of 0.005 to 0.008. Since a similar Ga content was determined in the starting materials (see section 4.1.1), Ga-contamination of the starting materials are the most reasonable explanations for this.

4.2   Semi-quantitative imaging of LLZO pellets

To investigate possible local variations in the chemical composition, two-dimensional distribution images of various LLZO garnets were created. Using LA-ICP-MS, sample surfaces of whole pellets were investigated. In addition, cross-sections of selected pellets were analyzed to reveal changes of the chemical composition within the samples.

Different LLZO garnets with an intended chemical composition of $Li_{6.4}Al_{0.2}La_3Zr_2O_{12}$ were analyzed. In the following section, the results of two such analyses are shown exemplary.

4.2.1   Sample "Al 0.20 Nr. 72"

For the creation of elemental distribution images of the LLZO sample "Al 0.20 Nr. 72", an area with the size of 7.0 x 6.9 mm was scanned using a laser beam with a diameter of 60 µm. The generated images are 117 x 115 pixels in size with a spatial resolution of 60 µm in both vertical and horizontal direction. The total acquisition time of the experiment was approximately 2 h.

A light micrograph taken before the laser ablation experiment is shown in Figure 24. The shining areas in the bottom right corner are the remains of a Pt coating used for conductivity measurements (not described in this work). This thin Pt film was removed completely during the Pre-ablation step.
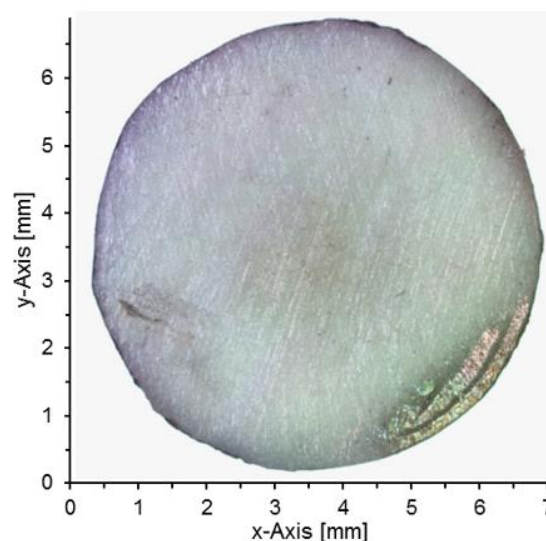
Figure 24: Light micrograph of the LLZO sample "Al 0.20 Nr. 72"

All signals were normalized to the intensity of the isotope ^{138}La to compensate differences in material ablation and instrumental drifts during measurement. The corresponding distribution images of Zr and Li are pictured in Figure 25 and Figure 26, respectively. In order to better illustrate the differences between various areas of the pellet, signal sequences along selected cross sections are displayed additionally. The cross sections were selected according to maximal signal variation.
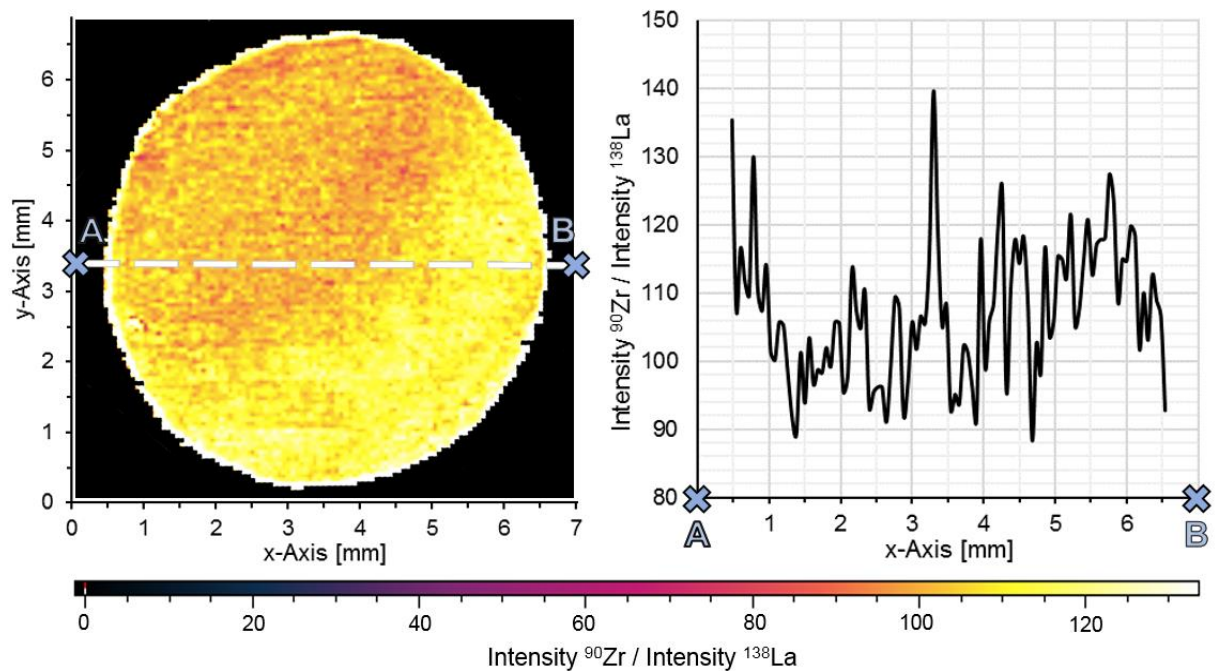
Figure 25: Zr/La distribution image of the LLZO sample "Al 0.20 Nr. 72" (117 x 115 pixels) and signal sequence along a selected cross-section
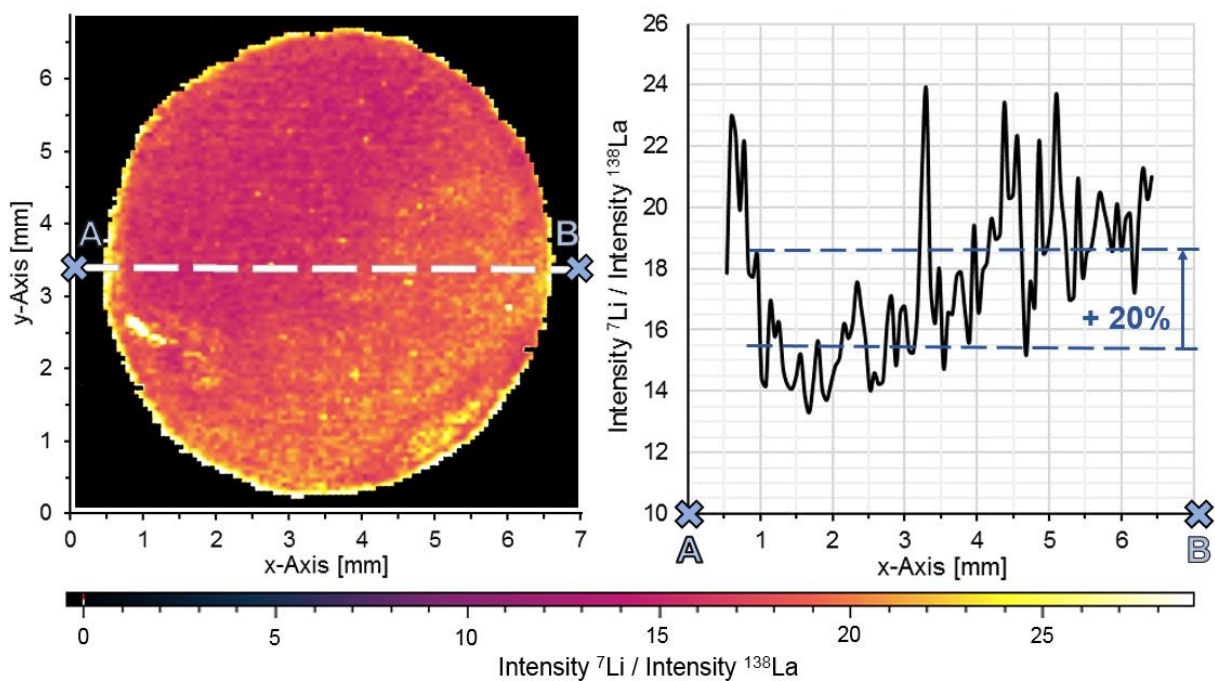
Figure 26: Li/La distribution image of the LLZO sample "Al 0.20 Nr. 72" (117 x 115 pixels) and signal sequence along a selected cross-section

No significant changes of the Zr/La ratio can be observed. Since it is unlikely that the Zr and La content change in the same ratio, this constant Zr/La ratio means that Zr as well as La are evenly distributed in the sample. The distribution image of the Li indicates small changes of the Zr/La ratio in the region of 20%. However, these changes are not significant, because the measurement uncertainty (variations between adjoining pixels) is greater than that.

In contrast to Zr and Li, a significant change of the Al and Ga content can be observed. The corresponding Images are shown in Figure 27 and Figure 28.
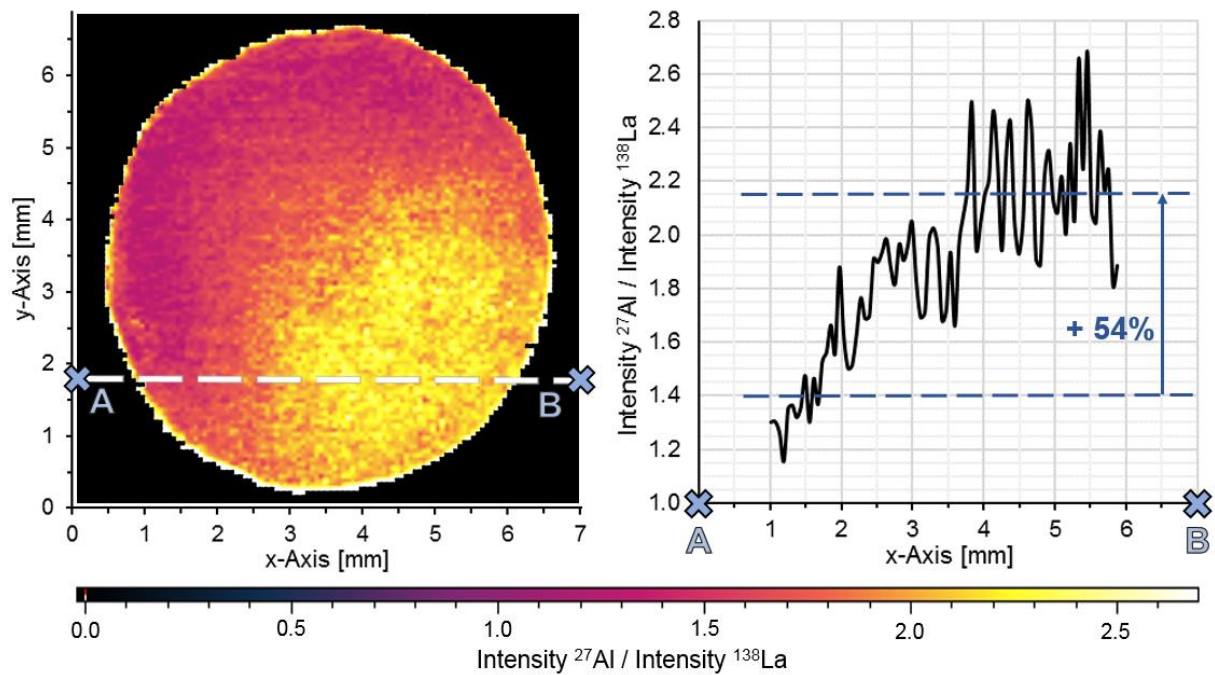
Figure 27: Al/La distribution image of the LLZO sample "Al 0.20 Nr. 72" (117 x 115 pixels) and signal sequence along a selected cross-section
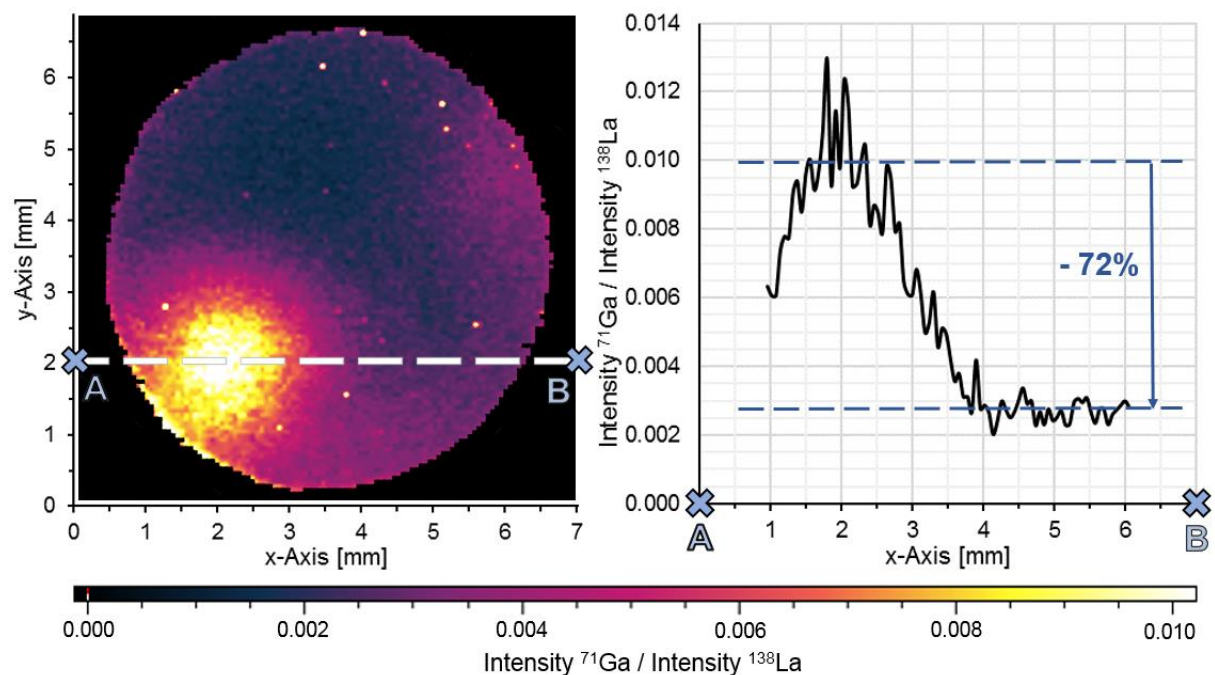
Figure 28: Ga/La distribution image of the LLZO sample "Al 0.20 Nr. 72" (117 x 115 pixels) and signal sequence along a selected cross-section

The images show an Al-enrichment in the bottom right and a Ga-enrichment in the bottom left corner of the pellet. For the Al/La ratio a variation of approximately 54% is observable, the Ga/La ratio changes even by approximately 72%.

Although quantification of LA-experiments is not possible without the measurement of appropriate standards, the Ga signal intensity can be compared to an element of similar mass to estimate the magnitude of the Ga contamination. Another prerequisite for this is that compared signals are free of significant background, which is fulfilled in this case. Considering the natural abundance of the measured isotopes, the greatest Ga signal is four orders of magnitude less than the corresponding Zr signal, which indicates a Ga mass fraction in the region of 0.002 wt%.

The measurements demonstrate that the chemical composition of LLZO pellets is subject to local variations. These inhomogeneities could be related to variable conduction behavior of different LLZO samples as well as to local conductivity variations. In addition, this finding reveals that sintered LLZO samples are not suitable for the use as calibration standards for LA experiments.

4.2.2   Sample "Al 0.20 Nr. 60"

Sample surface

Two-dimensional distribution images of the LLZO sample "Al 0.20 Nr. 60" were created by scanning an area with the size of 8.4 x 7.6 mm with a laser beam diameter of 60 µm, leading to images of 140 x 127 pixels in size.
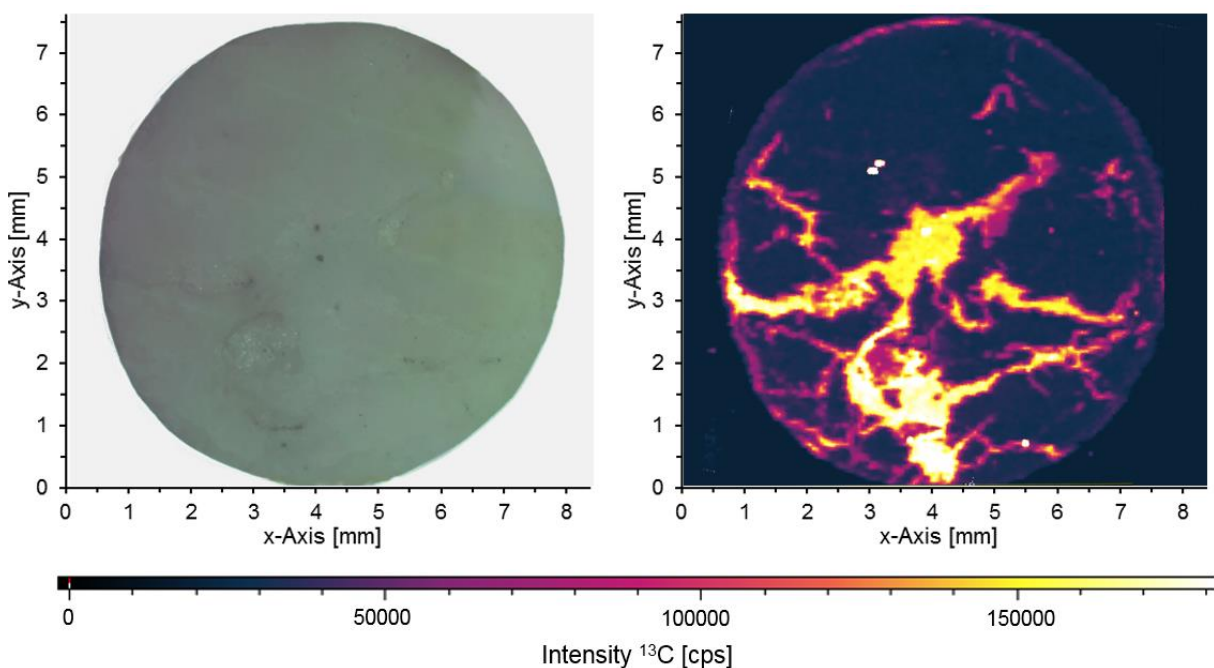
Figure 29: Light micrograph of the LLZO sample "Al 0.20 Nr. 60" and corresponding C-distribution image

In Figure 29 a light micrograph of the sample is compared to the corresponding C-distribution image without signal normalization. A high signal intensity is observable in large areas of the sample. Since contamination from the SiC grinding paper can be excluded due to a lack of Si signals in the corresponding regions, the origin of these C-rich phases remains unclear.

Since no significant amounts of Al, Ga, La, Li, or Zr were detected in the C-rich areas, these pixels were excluded for signal normalization and further image processing. The resulting Zr and Li images are shown in Figure 30 and Figure 31, respectively.
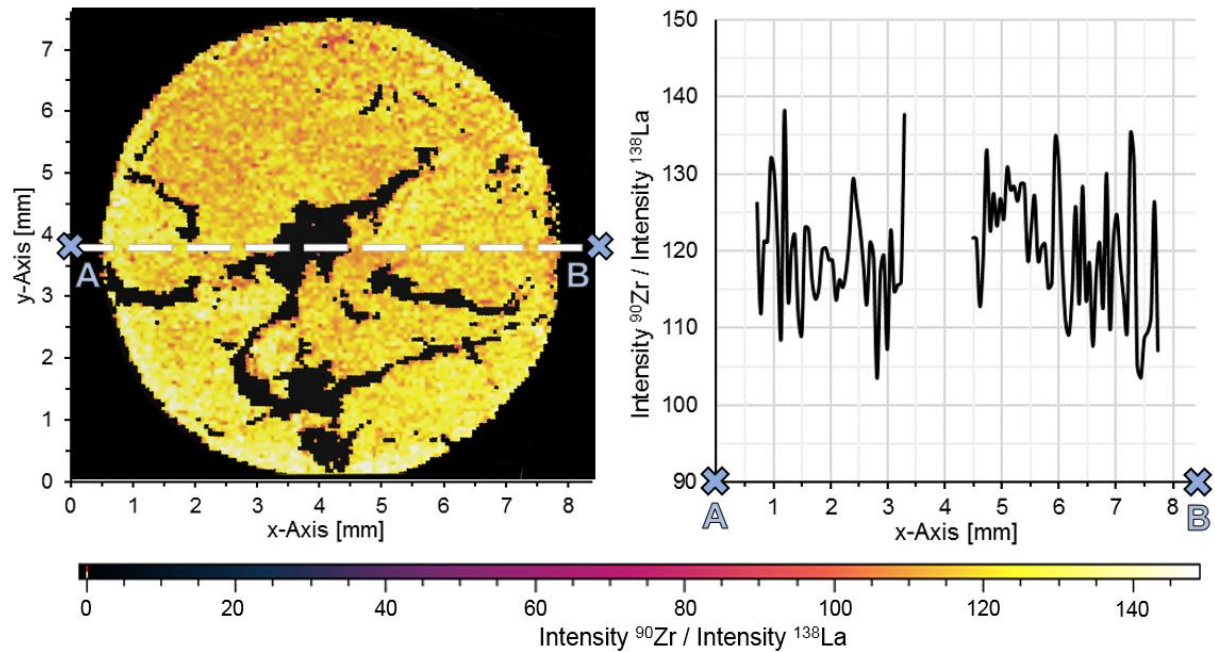
Figure 30: Zr/La distribution image of the LLZO sample "Al 0.20 Nr. 60" (140 x 127 pixels) and signal sequence along a selected cross-section
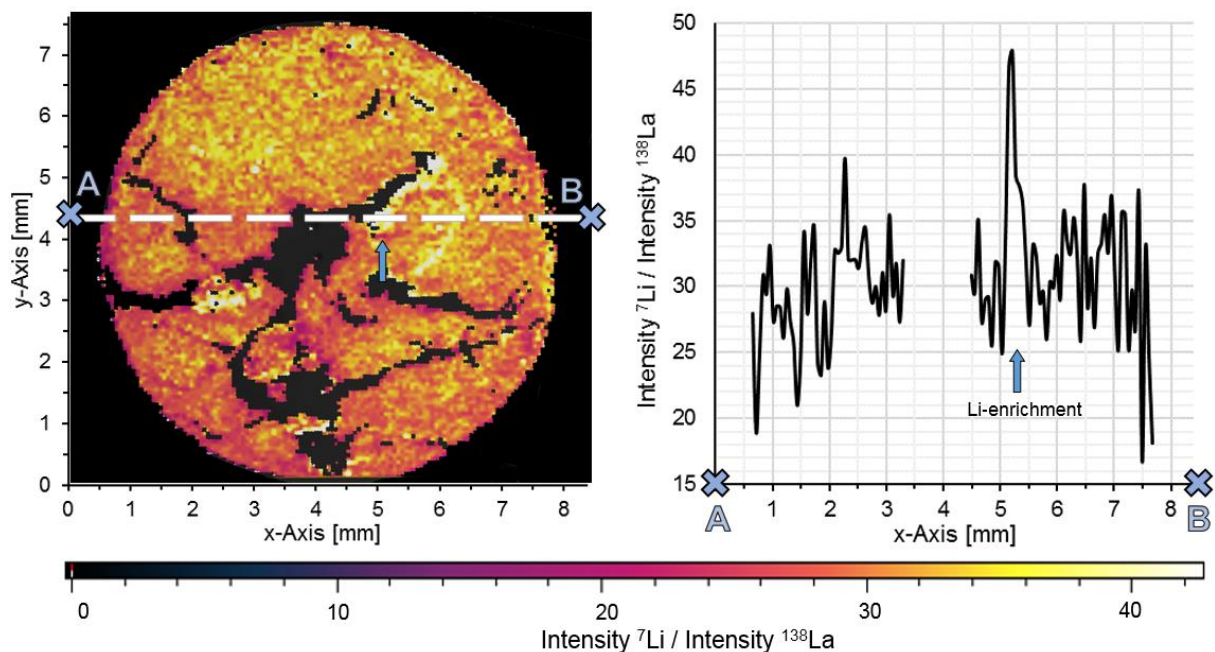
Figure 31: Li/La distribution image of the LLZO sample "Al 0.20 Nr. 60" (140 x 127 pixels) and signal sequence along a selected cross-section

A constant Zr/La ratio can be observed across the entire sample surface, which indicates that Zr as well as La are evenly distributed in the whole pellet.

Small areas with an increased Li content are visible in the Li-distribution image. These impurity phases have a size in the range of 200 to 500 µm and are mostly next to the C-rich phases. A possible reason of these impurities is the segregation of Li_2CO_3.

In Figure 32 and Figure 33 the Al- and Ga-distribution images of the LLZO sample are displayed. As in the analysis of the sample "Al 0.20 Nr. 72", local variations of the Al content as well as a Ga-enrichment are observable.
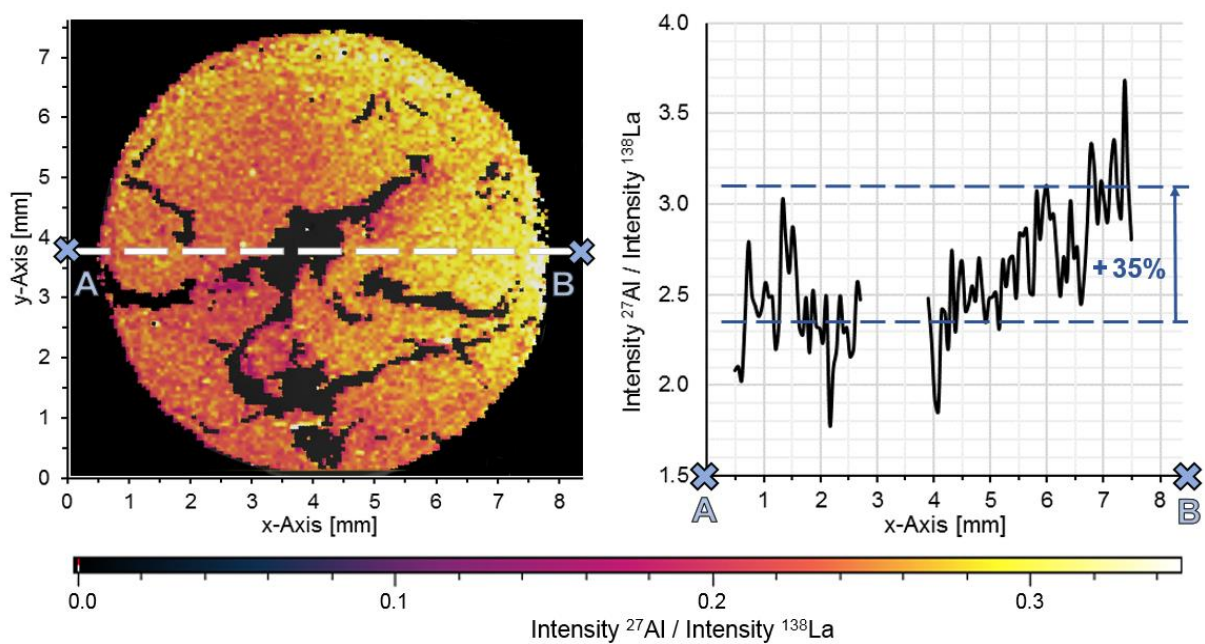
Figure 32: Al/La distribution image of the LLZO sample "Al 0.20 Nr. 60" (140 x 127 pixels) and signal sequence along a selected cross-section
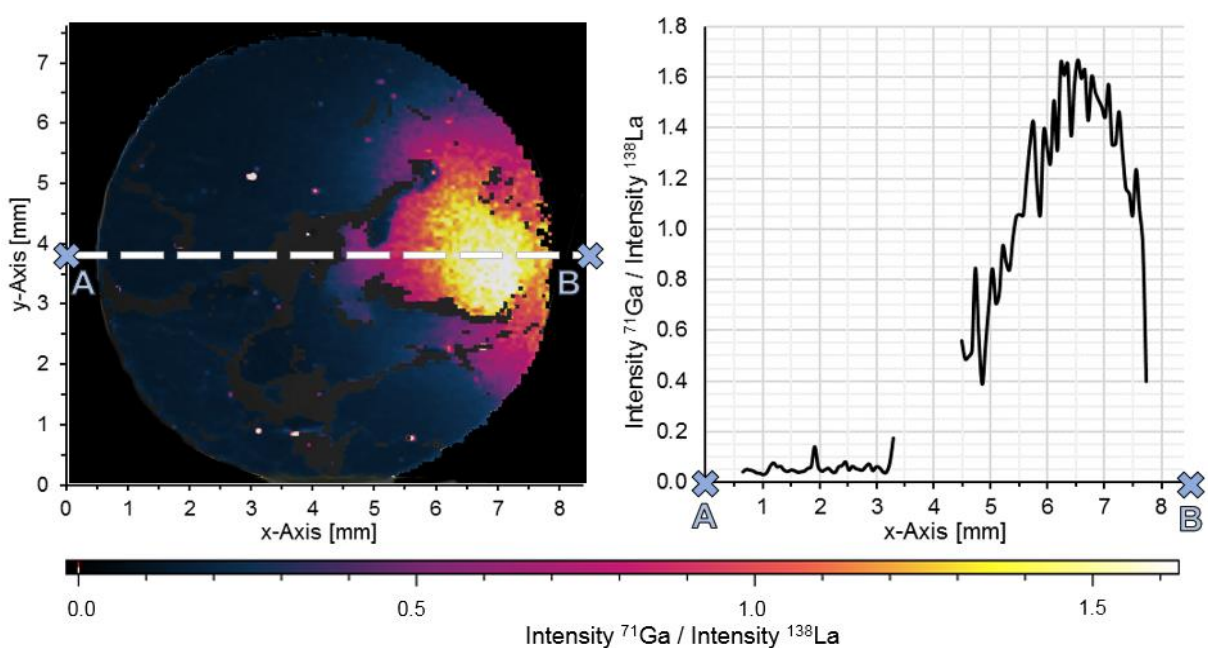
Figure 33: Ga/La distribution image of the LLZO sample "Al 0.20 Nr. 60" (140 x 127 pixels) and signal sequence along a selected cross-section

Due to the fact that the Ga-enrichments of both samples are very similar in terms of shape and position on the sample surface, a local Ga-contamination of the used pressing mold is a reasonable explanation for them. Compared to the Ga-enrichment on the sample "Al 0.20 Nr. 72", the Ga intensity for this sample is two orders of magnitude greater, which correlates to a Ga mass fraction in the magnitude of 0.2%.

Cross-section

In all distribution images shown so far, only the surface of the LLZO pellets was analyzed. To investigate changes of the chemical composition within the pellet, the sample "Al 0.20 Nr. 60" was cut in half along a plane perpendicular to the already scanned surface. The cross section exposed this way was then analyzed using similar laser settings. The corresponding micrograph and C-distribution image are shown in Figure 34. Like on the sample surface also within the pellet a C-rich phase can be observed.
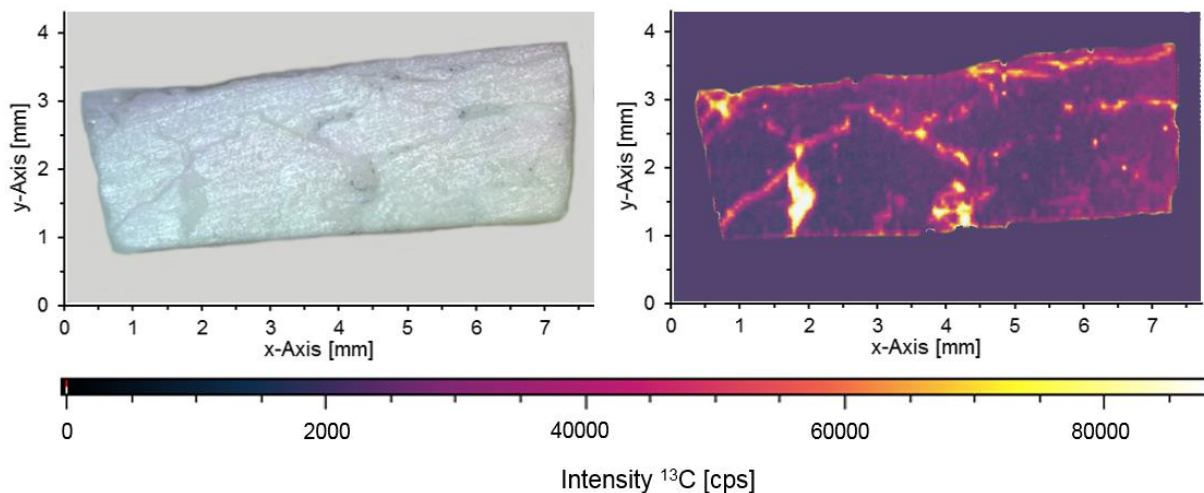
Figure 34: Light micrograph of the cross section of LLZO sample "Al 0.20 Nr. 60" and corresponding C-distribution image

The other measured elements also show a similar distribution within the sample as at the surface. The corresponding pictures are displayed in Figure 35 to Figure 38. A nearly constant Zr/La ratio as well as Li-rich areas and local variations of the Al content are observable.

The Ga-enrichment is only visible close to the sample surface in a depth up to approximately 250 µm. This confirms the theory of local Ga-contamination on the mold used for sample pressing.
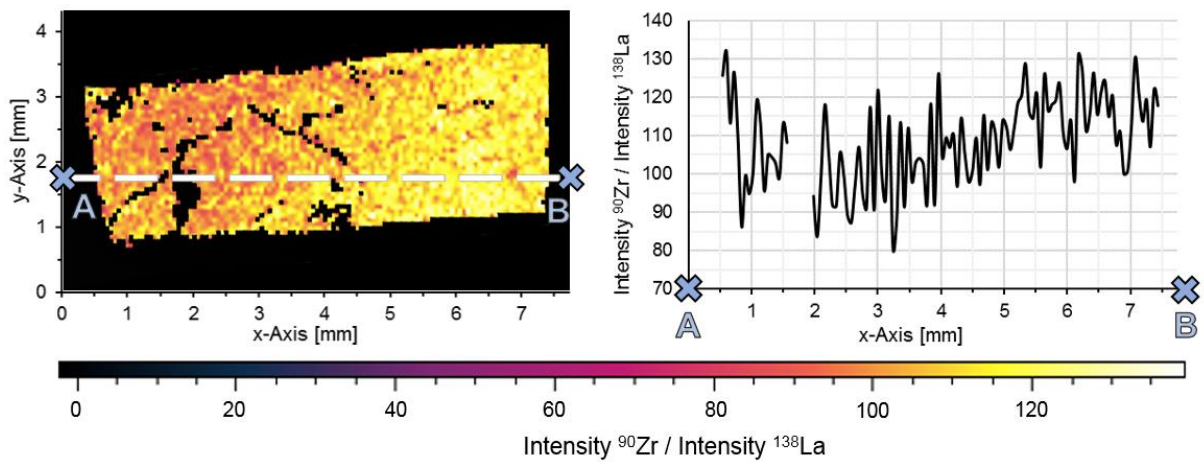
Figure 35: Zr/La distribution image of the cross section of LLZO sample "Al 0.20 Nr. 60"
(129 x 72 pixels)
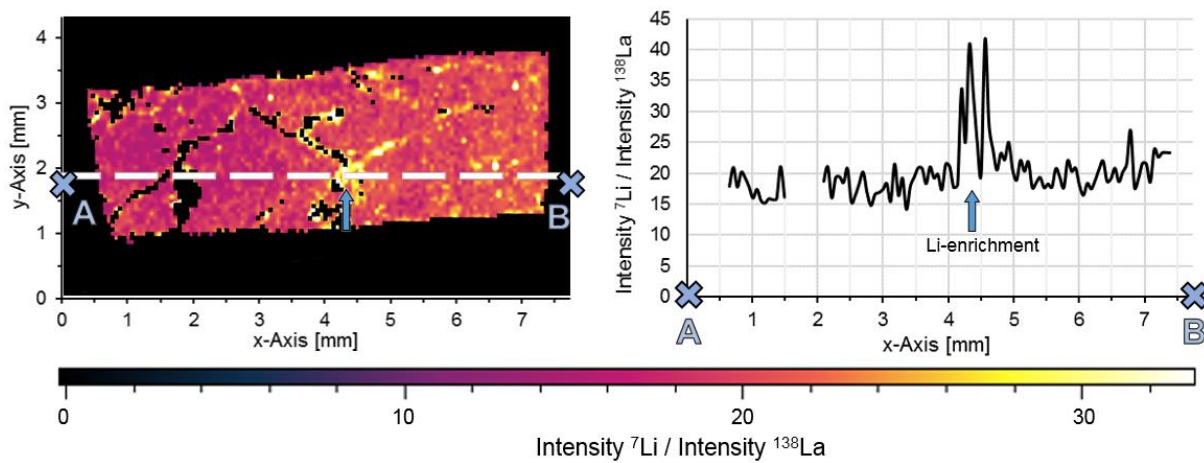
Figure 36: Li/La distribution image of the cross section of LLZO sample "Al 0.20 Nr. 60"
(129 x 72 pixels)
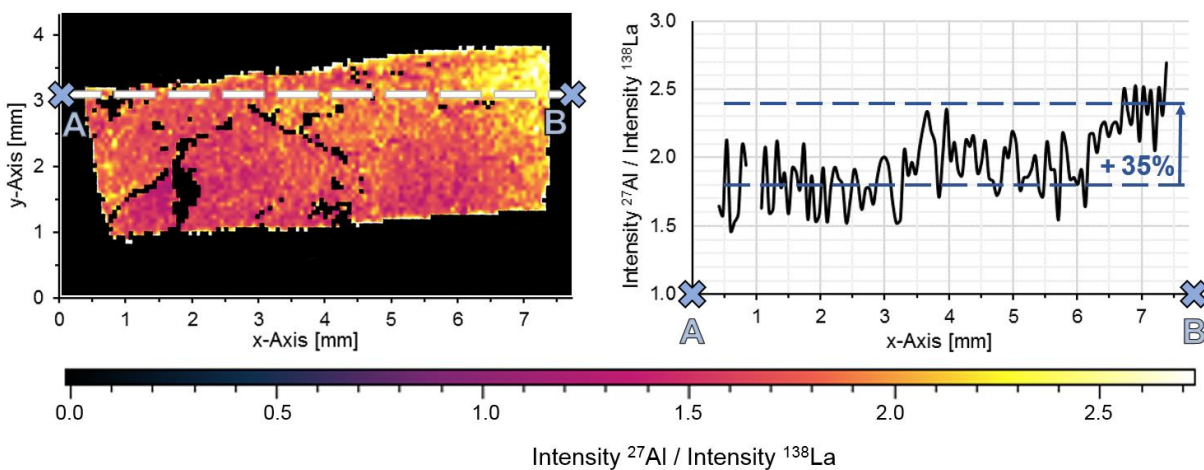
Figure 37: Al/La distribution image of the cross section of LLZO sample "Al 0.20 Nr. 60"
(129 x 72 pixels)
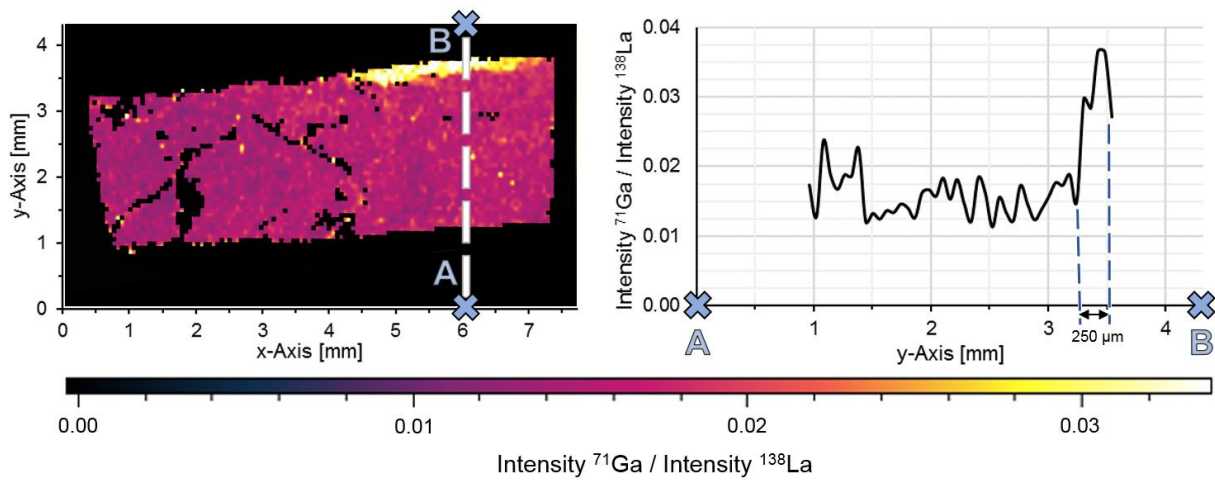
Figure 38: Ga/La distribution image of the cross section of LLZO sample "Al 0.20 Nr. 60" (129 x 72 pixels)

4.3   External calibration of LA experiments

Since matrix-matched standards are necessary to obtain reliable quantitative information from LA-ICP-MS and LA-ICP-OES measurements, LLZO standards with known chemical composition are required for the analysis of LLZO samples. Although sintered LLZO pellets would provide the perfect matrix, they are not suitable for the use as standards, because their chemical composition is not constant (see section 4.2.). Therefore, an elaborate approach is required.
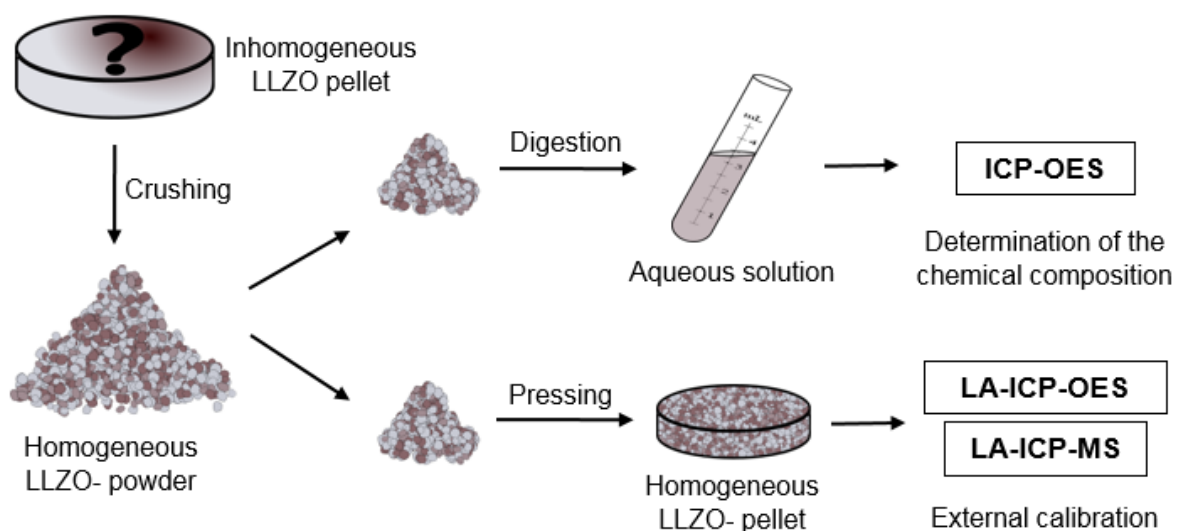
Figure 39: Strategy for the preparation of matrix-matched standards suitable for external calibration of LA measurements

The quantification strategy used for external calibration of LA-ICP-MS and LA-ICP-OES measurements is shown in Figure 39. The first step is crushing, grinding and homogenizing of sintered "$Li_{7-3x}Al_xLa_3Zr_2O_{12}$" pellets with varying Al content using an agate mortar. To determine the chemical composition of the resulting LLZO powders, a part of each sample was digested and analyzed by ICP-OES (see section 4.1.2). The other parts of the LLZO powders were pressed into pellets and used for LA measurements. Since the chemical compositions of these pellets are identical with those of the powders and therefore known, they can be used as calibration standards.

4.3.1   LA-ICP-MS

In a first approach, the prepared matrix-matched standards were used for external calibration of LA-ICP-MS analyses. For the measurement of these standards, each pressed pellet was analyzed using multiple ablations of four line scan patterns. To correct variations in sample ablation and transport as well as instrumental drifts, signal normalization was carried out using La as internal standard.

To ensure that the used ablation patterns are representative for the whole sample, the means of each pattern were compared using one-way ANOVA in the statistical software package DataLab (v.3.530, Epina, Austria). Because the statistical analysis did not indicate that the values differ significantly ($\alpha = 0.05$), the means of the individual patterns were averaged and the corresponding standard deviations calculated. The obtained results Al- and Li-calibration are shown in Figure 40.

The external calibration of the ^{27}Al signal shows a distinct linear correlation. The corresponding regression line features a high coefficient of determination R^2 of 0.999 and the replicate standard measurements show an average RSD below 6%. However, a significantly negative y-intercept can be observed. Such a phenomenon can be explained by analyte loss during the measurement, but this seems implausible for the performed experiments. Since no reasonable explanation for this unusual phenomenon could be found, a constant systematic error of the LA measurement and/or the ICP-OES analysis used for determination of the chemical composition of the standards must be assumed. This leads to questionable accuracy of the calibration, especially for LLZO samples with a low Al content. A possible reason for such a systematic error are spectral interferences in the ICP-OES analysis. Although there was no indication of a spectral interference in any form, it cannot be completely excluded due to the lack of a second suitable Al emission line.

For the normalized ^{7}Li signals no significant correlation can be observed. Compared to Al, getting useful regression line is a much harder task in case of Li, because the variations of the Li content are significantly smaller: While the highest Al mass fraction differs from the lowest one by a factor of 4, the corresponding values of the Li mass fraction differ only by about 15%. However, even in case of Li at least a rough trend should be observable for an interference-free measurement. This evident lack of precision of the LA-ICP-MS analysis can be explained by mass discrimination due to space-charge effects: The ion beam generated in the mass

spectrometer contains high charge density, which leads to electrostatic repulsion between the positively charges ions, forcing their trajectories away from the beam axis. Since the magnitude of this deviation depends on the mass of the ions, this effect particularly decreases the transmission of light ions. [29] Because the amount of ablated sample material is not constant during the LA measurement, also the charge density in the ion beam and thereby the magnitude of the space-charge effects varies, ultimately leading to a decrease of the precision of the analysis, particularly for light ions as Li^+.
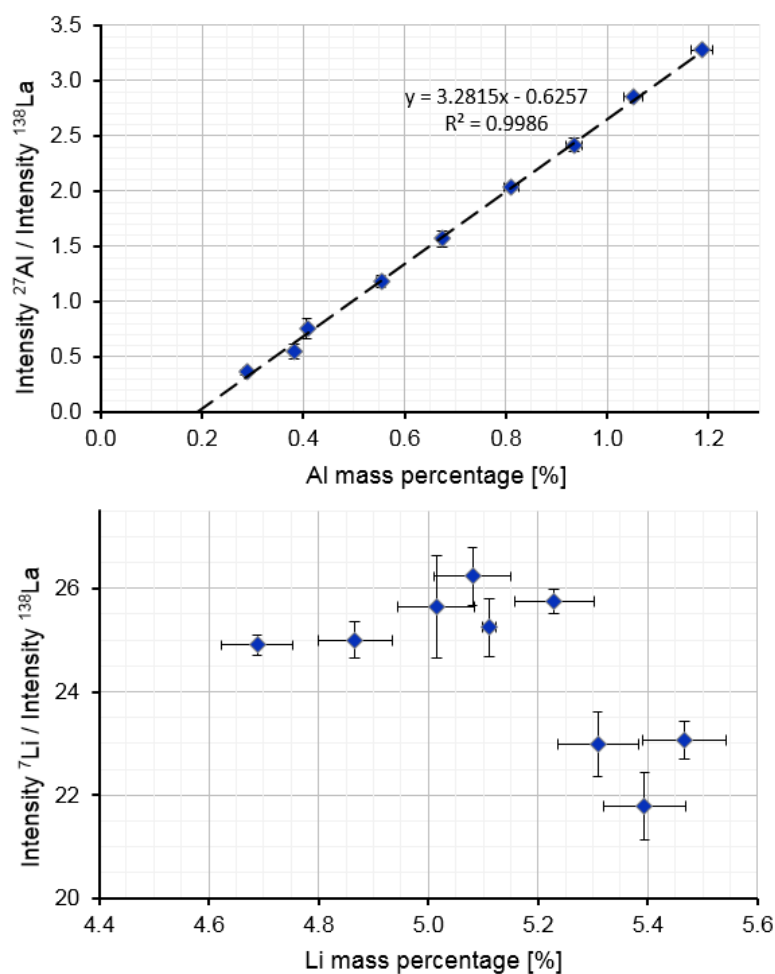
Figure 40: External LA-ICP-MS calibration of ^{27}Al and ^{7}Li using pressed LLZO pellets as matrix-matched standards and ^{138}La as internal standard for signal normalization. The vertical error bars represent the SDs derived from the measurement of multiple ablation patterns, the horizontal error bars represent the measurement uncertainty of the ICP-OES method used for standard characterization.

Since also the application of other calibration strategies including internal-standard independent 100 wt% normalization did not lead to any significant improvements of the results (data not shown), LA-ICP-MS seems not suitable for the quantitative analysis of LLZO samples.

4.3.2 LA-ICP-OES

To improve the precision of the Li-determination, LA measurement was used in combination with ICP-OES as an alternate approach. Since OES is based on the detection of emitted photons, space-charge effect should not limit the accuracy of the method.

As with the LA-ICP-MS measurements described in the previous section, each calibration standard was analyzed using multiple ablation patterns. Since statistical analysis by one-way ANOVA did not indicate that the means of the used ablation patterns differ significantly ($\alpha = 0.05$), these means were averaged for further data evaluation.

Two different calibration strategies were used for signal quantification: Conventional univariate external calibration using La as internal standard and an internal-standard independent 100 wt% normalization strategy presented by Liu et al. [13]

Calibration using La as internal standard

As a first approach for signal normalization La was used as internal standard assuming that the La content is equal in all standards and samples. The chemical analysis of the powders used for the preparation of the standards confirms this assumption is for all LLZO standards expect for the "Al 0.00" standard, which exhibits an about 2% lower Zr/La atomic ratio.

The obtained LA-ICP-OES regressions for the Al and Li signal are displayed in Figure 41. Compared to the LA-ICP-MS measurement, significant improvements of the calibrations can be observed. The linear regression of the Al signals shows a coefficient of determination above 0.999 and an average RSD of the measurement below 2%. Also for the LA-ICP-OES regression a negative y-intercept can be observed, however, the deviation of the expected zero-intercept is significantly decreased. As already discussed in section 4.3.1, a constant systematic error must be assumed because of the negative y-intercept. To estimate the inaccuracy caused by such an error, the measured regression line was compared to a regression line with identical slope but zero-intercept. The corresponding mass fractions differ in the range of 5% for the LLZO standard with the greatest Al content to 24% for the standard with the lowest Al concentration.

The LA measurement of Li features a low average RSD of 1.4% and a regression line with a coefficient of determination of 0.934. As already mentioned, obtaining a useful Li-calibration is difficult due to relative small variations of the Li contents of the LLZO pellets (the highest Li mass fraction differs from the lowest one only by about 15%). Therefore, the remaining deviations of perfect linear correlation can be explained by measurement uncertainties of the LA measurement and the ICP-OES analysis used for the characterization of the standards. Additionally, inaccuracies of the already mentioned assumption that the La content is equal in all standards lead to a certain error.
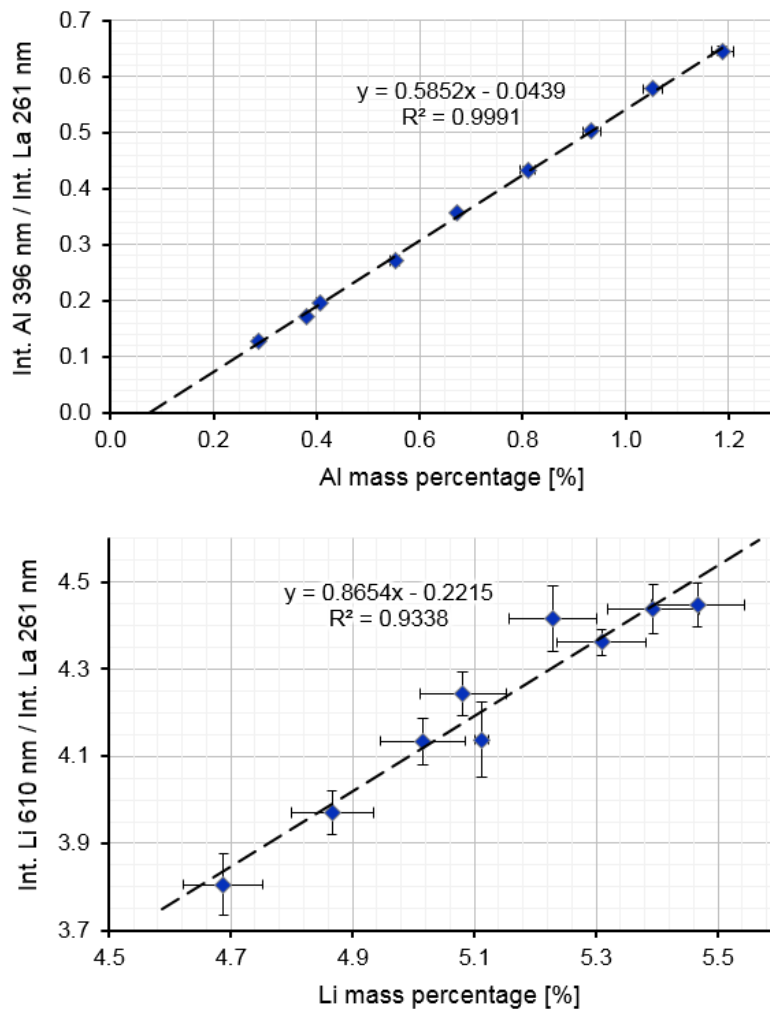
Figure 41: External LA-ICP-OES calibration of Al and Li using pressed LLZO pellets as matrix-matched standards and La as internal standard for signal normalization. The vertical error bars represent the SDs derived from the measurement of multiple ablation patterns, the horizontal error bars represent the measurement uncertainty of the ICP-OES method used for standard characterization.

Calibration using 100 wt% normalization

As a second normalization approach, a calibration strategy based on the normalization of the sum of all metal oxides to 100 wt% was applied. [13]

To determine the accuracy of the analysis in combination with this normalization strategy, the mass fractions of each standard were calculated using all other standards for calibration. The determined mass fractions were compared to the target values and the corresponding relative deviations were calculated. The results of this external validation are given in Figure 42.

Average relative deviations of about 3% can be observed for the La, Li, and Zr mass fractions. Since no deviation is greater than 6.5%, the used calibration strategy seems reliable for these elements.

The Al mass fractions show significantly greater deviations from the target values. An average relative deviation of 9.6% with a maximum value of nearly 18% can be observed. It can be assumed that the reasons for these significantly greater deviations are the same as those for the already discussed negative y-intercept of the external calibrations. However, compared to the other elements a greater relative measurement uncertainty hast to be expected for Al, because La, Li, and Zr are main constituents of LLZO and the Al content is not even1%.
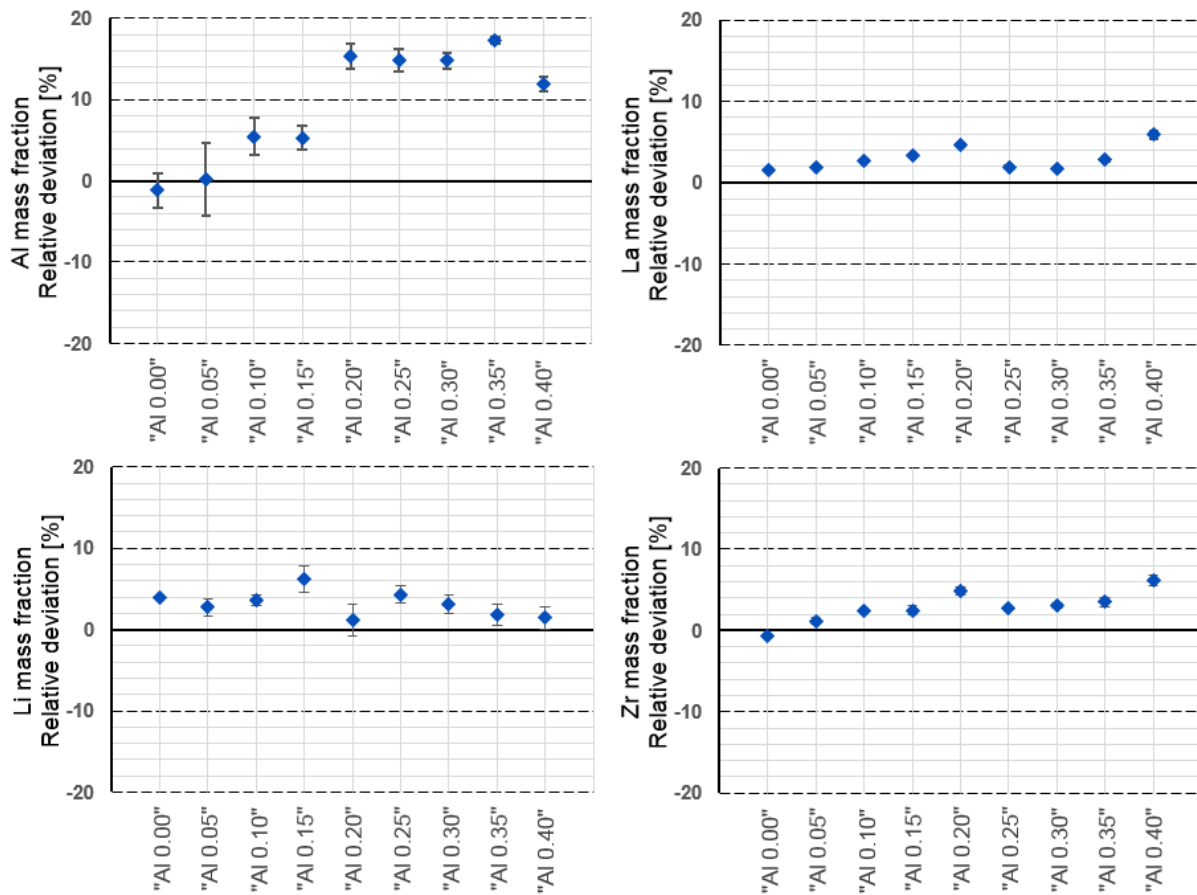
Figure 42: Relative deviations of the mass fractions determined by LA-ICP-OES and 100 wt% normalization from the target values. The error bars represent the RSDs of the analysis derived from the measurements of multiple ablation patterns.

The results show that most of the calculated mass fractions are greater than the corresponding target values. This can be explained by the fact that the used 100 wt% normalization model assumes that the samples consist solely of the oxides of the measured elements. Since this is not completely correct due to the possible presence of other cations (e.g., Ga^{3+}) or anions (e.g., CO_3^{2-}, OH^-) as well as other impurities (e.g., C), this calibration strategy tends to deliver increased values. Minor Ga-contaminations of the LLZO samples were determined in experiments already shown and were not considered for the LA-ICP-OES measurements. However, the detected Ga concentrations were below 0.2 wt% and should therefore not affect the results significantly.
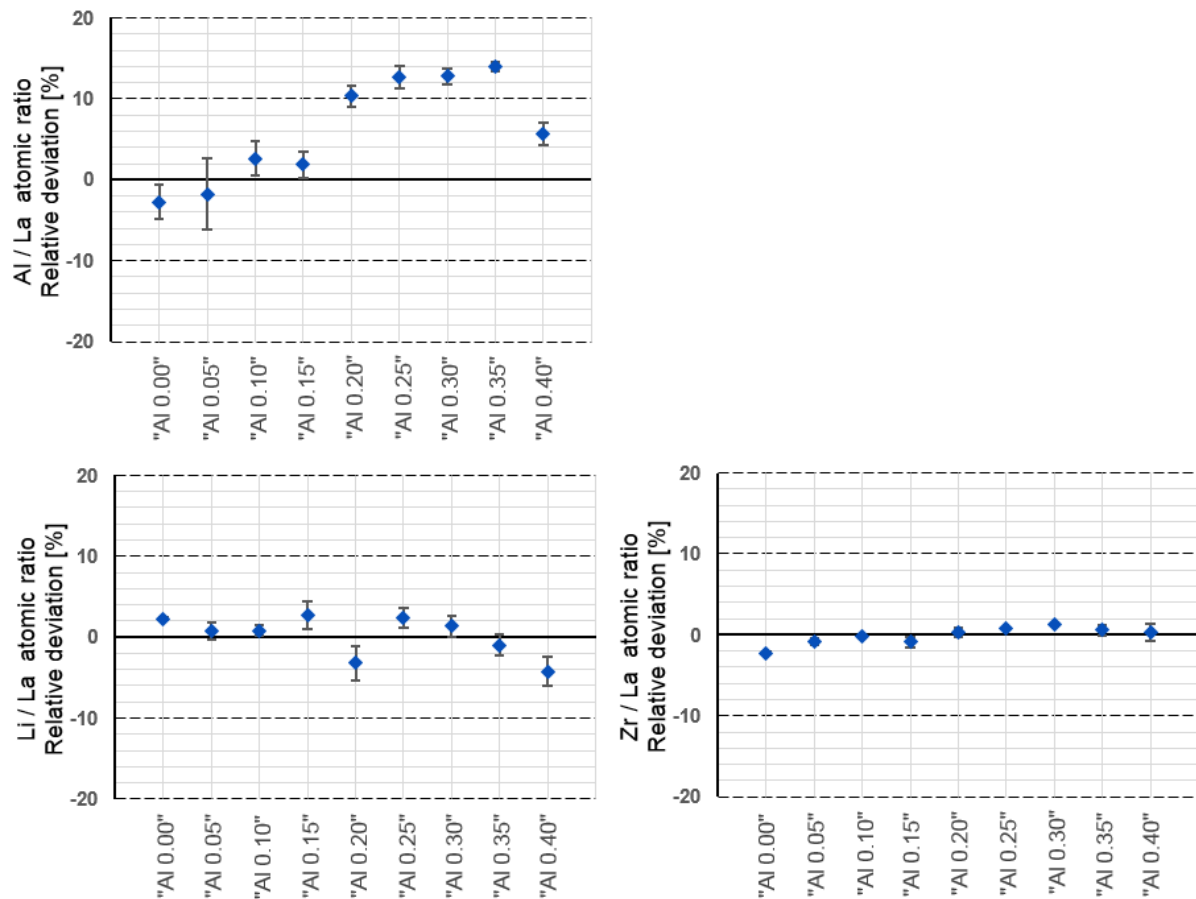
Figure 43: Relative deviations of the atomic ratios determined by LA-ICP-OES and 100 wt% normalization from the target values. The error bars represent the RSDs of the analysis derived from the measurements of multiple ablation patterns.

Since the calibration using 100 wt% normalization enables the determination of all measured elements, the corresponding atomic ratios can be calculated. The obtained results are shown in Figure 43.

Significant improvements of the calibrations can be observed. The average relative deviation for the Li/La and the Zr/La ratio decreased to 2.1 and 0.8%, respectively. With an average deviation of 7.2%, also an improvement of the Al-calibration is observable. The reduced deviations can be explained by the fact that the already mentioned inaccuracies caused by the 100 wt% assumption compensate each other partly when the element concentrations are set in relation to each other.

4.4 Quantitative and spatially resolved analysis of $Li_{7-3x}Al_xLa_3Zr_2O_{12}$ pellets

As shown in the previous section, the use of LA-ICP-OES provides much better results for the analysis of LLZO samples compared to the corresponding LA-ICP-MS measurements. Because of this, quantitative analysis of LLZO pellets was carried out using LA-ICP-OES only. Different LLZO samples with an intended chemical composition of $Li_{6.4}Al_{0.2}La_3Zr_2O_{12}$ were analyzed using the already described calibration strategies. In the following, the results of the analysis of the sample "Al 0.20 Nr. 89" are shown exemplary.

The LA measurement of the samples was carried out using single line scans across the whole LLZO pellets. To obtain lateral resolution, each line scan was divided into 10 s regions and each region was quantified individually.

4.4.1 La as internal Standard

Using conventional external calibration and La as internal standard was the first approach for signal quantification. Each region of the line scan was quantified using the calibrations shown in section 4.3.2 (see Figure 41). The obtained mass fractions of Al and Li are shown in Figure 44. Using the laser scan speed and the acquisition times, the position of each region was calculated and expressed as a longitude coordinate. The displayed error bars represent the standard deviations of the estimated mass fractions, which were calculated using Equation 3 and Equation 4.

$$s_x = \frac{s_y}{|m|} \cdot \sqrt{\frac{1}{n} + \frac{(y_{unk} - \bar{y})^2}{m^2 \cdot \sum_{i=1}^{n}(x_i - \bar{x})^2}} \qquad \text{Equation 3}$$

$$s_y = \sqrt{\frac{\sum_{i=1}^{n}(y_i - m \cdot x_i - b)^2}{n - 2}} \qquad \text{Equation 4}$$

s_x…standard deviation of estimated mass fraction
s_y…standard deviation in the residuals
m…slope of the regression line
b…y-intercept of the regression line
n…number of standards
y_i…intensity of standard i
$\bar{y}$…average intensity of the standards
y_{unk}…intensity of the sample
x_i…mass fraction of standard i
$\bar{x}$…average mass fraction of the standards
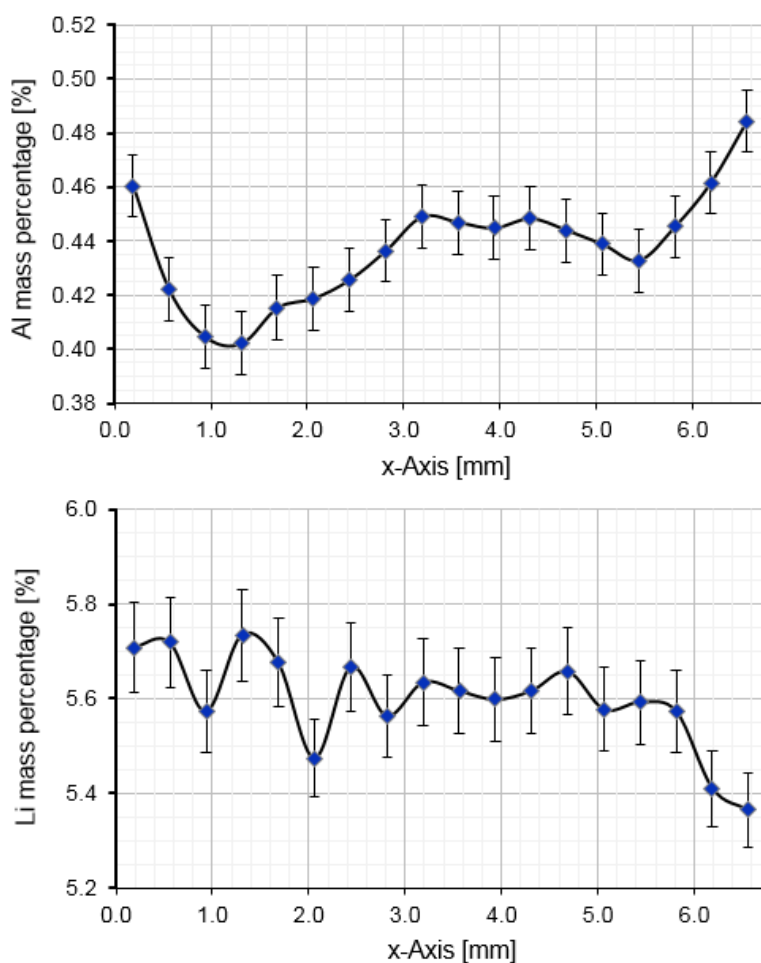
Figure 44: Lateral resolved Al and Li mass fractions of the LLZO sample "Al 0.20 Nr. 89" determined by LA-ICP-OES. Quantification was carried out using external calibration and La as internal standard. Error bars represent the standard deviations of the mass fractions calculated from the calibration curves.

To ensure that the La content of the sample matches the ones of the standards, the La/Zr ratios of the average signal intensities were compared. Since the relative deviation was less than 1.5%, it can be assumed that La as well as the Zr content of sample and standards are nearly equal. Furthermore, the La/Zr ratios of the individual regions were compared to ensure that La is distributed uniformly in the sample. No significant variations were observable.

The obtained Al contents vary between 0.40 and 0.49 wt%. A w-shaped concentration profile with the greatest Al concentrations near the edge of the pellet and as well as a relative maximum in the middle of the pellet can be observed. The RSDs of the estimated values are below 3%, which makes the spatial concentration changes significant.

The determined Li concentrations do not indicate a change of the Li content for most of the pellet. Only for the last two regions a significant decrease from 5.6 to 5.4 wt% can be observed. With an average RSD of 1.6% for the estimated mass fractions, the measurement uncertainty of the Li-determination is less than those of the Al-analysis. Although an increased Al content should result in a decreased Li content, no clear correlation of the corresponding mass fractions is observable.

4.4.2 100 wt% normalization

As a second approach for signal quantification, the described internal-standard independent calibration strategy based on 100 wt% normalization was applied. To ensure comparability, the same dataset was used for the evaluation. Also in this calibration approach, each region of the line scan was quantified individually.

The obtained mass fractions are shown in Figure 45. In case of Al and Li, the corresponding results of the quantification method using La as internal standard are plotted additionally. The displayed error bars represent the average relative deviation of the calibrations determined in section 4.3.2.
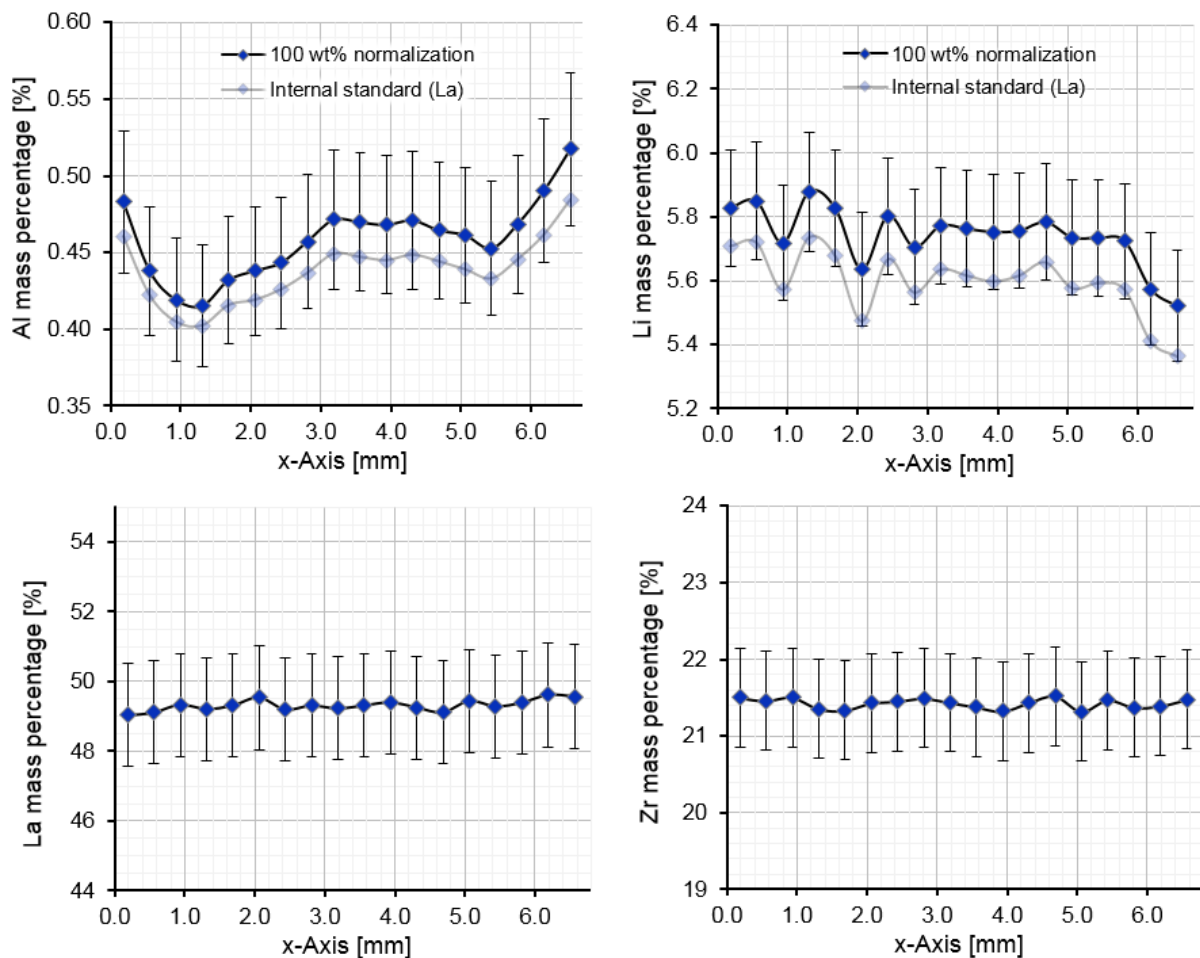
Figure 45: Lateral resolved mass fractions of the LLZO sample "Al 0.20 Nr. 89" determined by LA-ICP-OES. Quantification was carried out using the internal-standard independent calibration strategy based on 100 wt% normalization. Error bars represent the average relative deviation of the calibrations determined by external validation.

No significant variations of the Zr and La content can be observed. The obtained mass fractions of $21.4 \pm 0.1\%$ Zr and $49.3 \pm 0.2\%$ La are in expected range for LLZO samples.

For the Al and Li mass fractions, the results show a good consistency between the values obtained by the different calibration strategies. The relative deviations of the two approaches

are constantly about 2.5% in case of Li and between 3.9 and 6.4% in case of Al. It can be observed that mass fractions determined using 100 wt% normalization are consistently higher than the corresponding values of the conventional quantification. This can be explained by the tendency of the 100 wt% calibration strategy to increased values, which was already discussed in section 4.3.2.

Although both calibration strategies provide similar results for the mass fraction of Al and Li, the 100 wt% normalization approach features a major advantage: Because also the mass fractions of La and Zr can be calculated, the determination of the complete stoichiometry of the sample is possible. Therefore, the atomic ratios must be computed. The corresponding results are displayed in Figure 46.
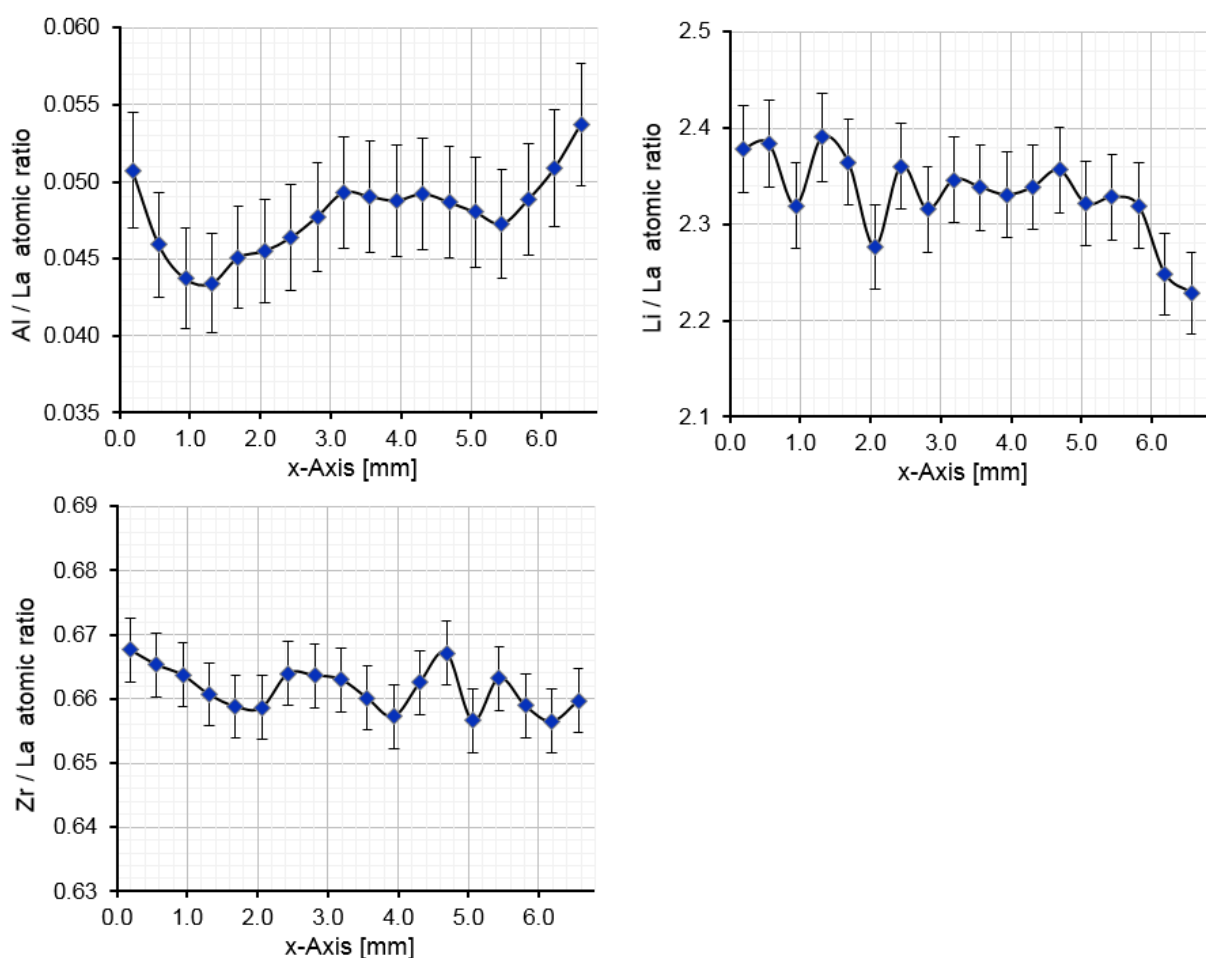
Figure 46: Lateral resolved atomic ratios of the LLZO sample "Al 0.20 Nr. 89" determined by LA-ICP-OES. Quantification was carried out using the internal-standard independent calibration strategy based on 100 wt% normalization. Error bars represent the average relative deviation of the calibration determined by external validation.

As expected, no significant variation of the Zr/La ratio is observable. With a determined value of 0.662 ± 0.003, the relative deviation from the intended value of 0.667 is less than 1%.

The Al/La and Li/La atomic ratios show a similar profile as the Al and Li mass fractions, respectively. As already mentioned in section 4.3.2, the measurement error is reduced when

the elements are set in relation to another, leading to relative deviations from the target values of 2.1% for Li/La and 7.2% for Al/La.

The results demonstrate that the developed LA-ICP-OES measurement using pressed LLZO pellets and the 100 wt% normalization is suitable for the direct solid analysis of $Li_{7-3x}Al_xLa_3Zr_2O_{12}$ garnets. Therefore, quantitative as well as laterally resolved information can be obtained.

5   Conclusion

Al-substituted LLZO ($Li_{7-3x}Al_xLa_3Zr_2O_{12}$) is one of the most promising candidates for a solid-state electrolyte to be used for future Li-based rechargeable batteries. To obtain a better understanding of the varying conduction behavior of different LLZO garnets as well as to investigate the processes involved in the synthesis, the determination of the chemical composition of LLZO samples is essential.

During this work, a reliable method for the bulk analysis of $Li_{7-3x}Al_xLa_3Zr_2O_{12}$ was developed. The use of borax fusion for sample digestion in combination with ICP-OES measurement enables the determination of the mass fractions of all LLZO-constituents expect for O with average RSDs below 4%.

The analyses of starting materials, intermediates and product of a "$Li_{6.4}Al_{0.2}La_3Zr_2O_{12}$" synthesis showed significant variations of the mass fractions of all elements, which can be explained by the loss/incorporation of CO_2 and/or moisture during the different stages of the synthesis process. Furthermore, a Ga concentration of 0.17 ± 0.02 wt% was detected in the starting materials, which was probably caused by contaminations of the oxides used for the synthesis.

Because of the mentioned fluctuations of the mass fractions, the comparison of the corresponding atomic ratios seems more suitable to determine changes of the chemical composition. Since the Li/La ratio of the finished sample is decreased by 8.9 ± 3.0% compared to the starting materials, it can be assumed that this fraction of Li has been lost during the sintering of the $Li_{6.4}Al_{0.2}La_3Zr_2O_{12}$ sample.

The analysis of different LLZO samples with varying Al contents indicates that the fraction of Li lost during sintering depends on the intended chemical composition of the garnet. However, no data of the corresponding starting materials is available to verify that result. Furthermore, the measurements indicate that a significant amount of Al is incorporated during sintering for samples with an intended Al content close to zero. An Al/La atomic ratio of 0.04 was determined for the theoretically Al-free LLZO sample.

By coupling of ICP-OES or -MS to laser ablation, spatially resolved direct solid analysis of LLZO was successfully carried out. Two-dimensional elemental distribution images of whole $Li_{6.4}Al_{0.2}La_3Zr_2O_{12}$ pellets obtained by LA-ICP-MS showed local variations of the Al content on the sample surface as well as within the pellet. Differences of the Al intensity up to relatively 54% were determined. In contrast to that, Zr as well as La seemed evenly distributed in the samples.

C-impurities as well as Li-rich phases were detected in some garnets. The latter were probably caused by the segregation of Li_2CO_3, however, the reason for the appearing C-phases remains unclear. Furthermore, Ga-enrichments were observed on different LLZO pellets. The magnitude of these contaminations was approximated semi-quantitatively, which yields to values of maximal 0.02 wt%. Since the Ga-enrichments were very similar in terms of shape and position on the sample surface and were only visible in a depth up to approximately 250 µm, they were probably caused by a local Ga-contamination of the mold used for pressing during the synthesis.

For the reliable signal quantification of LA-experiments, matrix-matched standards with homogeneous chemical composition are required. During this work, appropriate $Li_{7-3x}Al_xLa_3Zr_2O_{12}$ standards were successfully prepared by pressing homogenized LLZO powders with varying Al content into pellets.

The external calibration of LA-ICP-MS measurements showed a distinct linear correlation for the Al signals. However, since a significantly negative y-intercept was observable and no explanation for this could be found, a constant systematic error must be assumed. Furthermore, a quantification of the Li signals was impossible, because no correlation between the signal intensity and the Li concentration was observable. This can be explained by mass discrimination due to space-charge effects, which results in a decrease of the precision of the analysis, particularly for light ions as Li^+. Because of this reasons, LA-ICP-MS seems not suitable for the quantitative analysis of LLZO samples.

In contrast to that, the external calibration of the LA-ICP-OES signals provides reliable results. With the use of La as an internal standard for signal normalization, suitable regression lines for Al ($R^2 = 0.999$) as well as for Li ($R^2 = 0.934$) with average RSDs of the measurements below 2% were obtained. Although also for the LA-ICP-OES Al regression line a negative y-offset was observable, the deviation of the expected zero-intercept was significantly decreased. A maximum error caused by this phenomenon of 0.075 wt% Al was estimated, which corresponds to a relative deviation between 5 to 24% depending on the Al content of the sample.

By applying an internal-standard independent calibration strategy based on the normalization of the sum of all metal oxides to 100 wt%, the mass fraction of all measured elements can be determined. This enables the calculation of the corresponding atomic ratios and thus, the stoichiometry determination of LLZO samples. The accuracy of the LA-ICP-OES analysis in combination with this calibration approach was estimated using the LLZO standards for external validation. For the Li/La, Al/La, and Zr/La atomic ratios relative deviations of 2.1%, 7.2%, and 0.8% were obtained, respectively.

The analysis of different LLZO pellets showed that the developed LA-ICP-OES method is suitable for the quantitative and laterally resolved analysis of $Li_{7-3x}Al_xLa_3Zr_2O_{12}$ garnets. The use conventional external calibration enables the estimation of the Al- and Li-mass fractions with RSDs below 3%. In case of Li, even an average RSD of 1.6% was obtained. Applying the 100 wt% normalization strategy provides similar results for the Al and Li content, however, the capability of complete stoichiometry determination makes this calibration strategy superior to the conventional approach.

In summary, a reliable method for the direct solid analysis of $Li_{7-3x}Al_xLa_3Zr_2O_{12}$ garnets was developed. Using LA-ICP-OES in combination with pressed pellets as matrix-matched standards and a 100 wt% normalization approach enables latterally resolved stoichiometry determination, without the need of time-consuming sample preparation. This provides relevant information contributing to a deeper understanding of the processes involved in the LLZO synthesis as well as the relationship between chemical composition and conduction behavior of LLZO garnets.

6   Outlook

Since the developed ICP-based methods enable the determination of stoichiometric variations of LLZO samples, further work will be directed on the influence of these variations on the conduction behavior of the garnets. Thereby, not only the overall Li-conductivity of LLZO pellets is of interest. By employing spatially resolved impedance spectroscopy, in which microelectrode measurements are used to obtain information on the conductivity, correlations between local variations of the stoichiometry and local conductivities can be investigated.

Further improvement of the accuracy of the measurements is also of great interest. Since the error of the Al-determination is mostly caused by a potential constant systematic error of unknown origin, upcoming experiments will be focused on the clarification of this phenomenon. Additionally, further work will be directed on the improvement of the spatially resolution of the stoichiometry determination. During the presented experiments, only laser ablation measurements using a laser beam diameter of 200 µm have been quantified. Since only macroscopic variations of the chemical composition can be observed using this set-up, an improved laterally resolution could enable new applications of the method.

Although Al is one of the most promising candidates for the doping of LLZO, also other supervalent cations including Ga, Ta, and Nb have been successfully used for the synthesis of high conductivity LLZO. [10, 30, 31] Therefore, implementing the established method for other dopants as well would enable the analysis of a greater variety of LLZO samples.

List of figures

List of tables

Literature

[1] J. M. Tarascon, M. Armand, *Issues and Challenges facing Rechargeable Lithium Batteries*. Nature, 2001, 414: p. 359-367.

[2] K. Xu, *Nonaqueous Liquid Electrolytes for Lithium-Based Rechargeable Batteries*. Chemical Reviews, 2004, 104 (10): p. 4303-4418.

[3] V. Thangadurai, S. Narayanan, D. Pinzaru, *Garnet-type solid-state fast Li ion conductors for Li batteries: critical review*. Chem. Soc. Rev., 2014, 43: p. 4714-4727.

[4] R. Murugan, V. Thangadurai, W. Weppner, *Fast Lithium Ion Conduction in Garnet-Type Li7La3Zr2O12*. Angew. Chem. Int. Ed., 2007, 46: p. 7778-7781.

[5] V. Thangadurai, D. Pinzaru, S. Narayanan, A. K. Baral, *Fast Solid-State Li Ion Conducting Garnet-Type Structure Metal Oxides for Energy Storage*. J. Phys. Chem. Lett., 2015, 6: p. 292-299.

[6] J. Awaka, N. Kijima, H. Hayakawa, J. Akimoto, *Synthesis and structure analysis of tetragonal Li7La3Zr2O12 with the garnet-related type structure*. Journal of Solid State Chemistry, 2009, 182: p. 2046-2052.

[7] J. Awaka et al., *Crystal Structure of Fast Lithium-ion-conducting Cubic Li7La3Zr2O12*. Chem. Lett., 2010, 40: p. 60-62.

[8] H. Buschmann et al., *Structure and dynamics of the fast lithium ion conductor "Li7La3Zr2O12"*. Phys. Chem. Chem. Phys., 2011, 13: p. 19378-19392.

[9] C. A. Geiger et al., *Crystal Chemistry and Stability of "Li7La3Zr2O12" Garnet: A Fast Lithium-Ion Conductor*. Inorg. Chem., 2011, 50: p. 1089-1097.

[10] J. Wolfenstine et al., *Synthesis and high Li-ion conductivity of Ga-stabilized cubic Li7La3Zr2O12*. Material Chemistry and Physics, 2012, 134: p. 571-575.

[11] A. Limbeck et al., *Recent advances in quantitative LA-ICP-MS analysis: challenges and solutions in the life sciences and environmental chemistry*. Anal Bioanal Chem, 2015, 407: p. 6593-6617.

[12] R. E. Russo et al., *Laser ablation in analytical chemistry - a review*. Talanta, 2002, 57: p. 425-451.

[13] Y. Liu et al., *In situ analysis of major and trace elements of anhydrous minerals by LA-ICP-MS without applying an internal standard*. Chemical Geology, 2008, 257: p. 34-43.

[14] N. Bernstein, M. D. Johannes, K. Hoang, *Origin of the Structural Phase Transition in Li7La3Zr2O12*. Phys. Rev. Lett., 2012, 109: p. 205702.

[15] X. Hou, B. T. Jones, *Inductively Coupled Plasma/Optical Emission Spectrometry* in *Encyclopedia of Analytical Chemistry*, (Ed: R. A. Meyers), p. 9468-9485, John Wiley & Sons Ltd, Chichester 2000.

[16] D. A. Skoog, F. J. Holler, S. R. Crouch, *Instrumentelle Analytik: Grundlagen - Geräte - Anwendungen.* 6th ed., Springer Spektrum, Berlin 2013.

[17] S. J. Hill, *Inductively Coupled Plasma Spectrometry and its Applications.* 2nd ed., Analytical Chemistry, Blackwell Publishing Ltd, Plymouth 2007.

[18] K. Cammann, *Instrumentelle Analystische Chemie.* 1st ed., Spektrum Akademischer Verlag, Heidelberg 2001.

[19] F. M. Dunnivant, J. W. Ginsbach, *Flame Atomic Absorbance and Emission Spectrometry and Inductively Coupled Plasma - Mass Spectrometry.* Whitman College Chemistry Department, Walla Walla 2009.

[20] Q. S. Hanley et al., *Charge-Transfer Devices in Analytical Instrumentation.* Analytical Chemistry News & Features, 1996, November 1: p. 661-667.

[21] A. A. Ammann, *Inductively coupled plasma mass spectrometry (ICP MS): a versatile tool.* J. Mass Spectrom., 2007, 42: p. 419-427.

[22] D. Günther, B. Hattendorf, *Solid sample analysis using laser ablation inductively coupled plasma mass spectrometry.* Trends in Analytical Chemistry, 2005, 24 (3): p. 255-265.

[23] K. L. Linge, K. E. Jarvis, *Quadrupole ICP-MS: Introduction to Instrumentation, Measurement Techniques and Analytical Capabilities.* Geostandards and Geoanalytical Research, 2009, 33 (4): p. 445-467.

[24] J. Pisonero, B. Fernández, D. Günther, *Critical revision of GD-MS, LA-ICP-MS and SIMS as inorganic mass spectrometric techniques for direct solid analysis.* J. Anal. At. Spectrom., 2009, 24: p. 1145-1160.

[25] S. F. Durrant, *Laser ablation inductively coupled plasma mass spectrometry: achievements, problems, prospects.* J. Anal. At. Spectrom., 1999, 14: p. 1385-1403.

[26] A. M. Leach, G. M. Hieftje, *Methods for shot-to-shot normalization in laser ablation with an inductively coupled plasma time-of-flight mass spectrometer.* Anal. At. Spectrom., 2000, 15 (9): p. 1121-1124.

[27] R. Wagner et al., *Crystal Structure of Garnet-Related Li-Ion Conductor Li7−3xGaxLa3Zr2O12: Fast Li-Ion Conduction Caused by a Different Cubic Modification?* Chem. Mater., 2016, 28: p. 1861-1871.

[28] L. Cheng et al., *The origin of high electrolyte–electrode interfacial resistances in lithium cells containing garnet type solid electrolytes*. Phys. Chem. Chem. Phys., 2014, 16: p. 18294-18300.

[29] H. Niu, R. S. Houk, *Fundamental aspects of ion extraction in inductively coupled plasma mass spectrometry*. Spectrochimica Acta Part B, 1996, 51: p. 779-815.

[30] Y. Li et al., *High lithium ion conduction in garnet-type Li6La3ZrTaO12*. Electrochemistry Communications, 2011, 13: p. 1289–1292.

[31] S. Ohta, T. Kobayashi, T. Asaoka, *High lithium ionic conductivity in the garnet-type oxide Li7−X La3(Zr2−X, NbX)O12 (X = 0–2)*. Journal of Power Sources, 2001, 196: p. 3342-3345.